Nano Today 28 (2019) 100767

Contents lists available at ScienceDirect

Nano Today

journal homepage: www.elsevier.com/locate/nanotoday

Review

Recent advances in synthesizing metal nanocluster-based nanocomposites for application in sensing, imaging and catalysis

Li Shang[a,b,**], Jie Xu[a], Gerd Ulrich Nienhaus[c,d,e,f,*]

[a] State Key Laboratory of Solidification Processing, Center for Nano Energy Materials, School of Materials Science and Engineering, Northwestern Polytechnical University, Xi'an, 710072, China
[b] NPU-QMUL Joint Research Institute of Advanced Materials and Structures (JRI-AMAS), Northwestern Polytechnical University, Xi'an, 710072, China
[c] Institute of Applied Physics, Karlsruhe Institute of Technology (KIT), 76131 Karlsruhe, Germany
[d] Institute of Nanotechnology, Karlsruhe Institute of Technology (KIT), 76344 Eggenstein-Leopoldshafen, Germany
[e] Institute of Toxicology and Genetics, Karlsruhe Institute of Technology (KIT), 76344 Eggenstein-Leopoldshafen, Germany
[f] Department of Physics, University of Illinois at Urbana-Champaign, Urbana, IL, 61801, USA

ARTICLE INFO

Article history:
Received 21 March 2019
Received in revised form 17 June 2019
Accepted 13 August 2019
Available online 23 August 2019

Keywords:
Metal nanoclusters
Nanocomposites
Sensing
Imaging
Catalysis

ABSTRACT

Metal nanoclusters (NCs) are a type of ultrasmall nanomaterials with unique physicochemical properties. Novel nanocomposites with exciting new and sometimes exotic properties can be created by combination of metal NCs with other functional materials, greatly expanding the range of possible applications. To exploit this potential, intensive research efforts have been made in recent years, resulting in a wide range of metal NC-based nanocomposites. In this review, we systematically summarize different strategies of fabricating nanocomposites and illustrate their application in sensing, imaging and catalysis. A brief outlook on the future development of metal NC-based nanocomposites is also presented.
© 2019 Elsevier Ltd. All rights reserved.

Contents

Introduction 2
Distinct properties of metal NCs 2
Synthesis approaches of metal NC-based nanocomposites 4
Chemical conjugation 4
Electrostatic interactions 4
Self-assembly 4
Ligand exchange 8
In-situ synthesis 8
Application of metal NC-based nanocomposites 9
Sensing 9
Luminescence sensing 9
ECL sensing 11
Colorimetric sensing 11
Electrochemical sensing 13
Bioimaging 13
In vitro luminescence imaging 13
In vivo luminescence imaging 14

* Corresponding author at: Institute of Applied Physics, Karlsruhe Institute of Technology (KIT), 76131 Karlsruhe, Germany.
** Corresponding author at: State Key Laboratory of Solidification Processing, Center for Nano Energy Materials, School of Materials Science and Engineering, Northwestern Polytechnical University, Xi'an, 710072, China.
E-mail addresses: li.shang@nwpu.edu.cn (L. Shang), uli@uiuc.edu (G.U. Nienhaus).

https://doi.org/10.1016/j.nantod.2019.100767
1748-0132/© 2019 Elsevier Ltd. All rights reserved.

In vivo multimodal imaging 15
Catalysis 17
Conclusions and outlook 20
Acknowledgements 20
References 20

Introduction

The past decades have witnessed a rapid advancement of nanoscience and nanotechnology [1–3]. It is now well recognized that, apart from biological nanomaterials, *e.g.*, proteins and nucleic acids, many other materials such as metals, semiconductors, salts and metal oxides can be engineered into nanomaterials. A multitude of chemical and physical approaches have been developed for the controlled synthesis of nanomaterials, including chemical/physical vapor deposition [4], mechanical grinding [5], hydrothermal synthesis [6], electrodeposition [7], laser ablation [8] and template synthesis [9]. The most fascinating aspect about nanomaterials is the emergence of size-dependent physicochemical properties that are distinctly different from those of their bulk counterparts. When the dimensions of materials are reduced to the nanometer scale, interesting new properties such as the quantum size effect and surface effects appear [10]. For example, metal nanoparticles (NPs), a well-studied class of nanomaterials, are known to exhibit strongly size-dependent optical, electronic and chemical properties, making them attractive for use in many different fields including biology [11], medicine [12,13], food [14], catalysis [15], environment [16] and information [17].

Metal nanoclusters (NCs), consisting of several to tens of atoms, have recently emerged as a new class of functional materials and attracted a great deal of interest [18,19]. With a core size of less than 2 nm, they bridge the gap between metal atoms and plasmonic NPs (Fig. 1). Unlike larger metal NPs, which possess continuous or semi-continuous energy levels, metal NCs exhibit discrete electronic structures. As a result, they display many intriguing molecule-like characteristics, such as enhanced photoluminescence [19], HOMO–LUMO transition [20], molecular chirality [21], magnetism [22] and discrete redox behavior [23]. Researchers have developed various strategies to synthesize metal NCs in a highly controlled manner so that different core sizes, chemical compositions, surface ligands and emission colors can easily be obtained. Various types of metal NCs, including AuNCs, AgNCs, CuNCs, AuAg alloy NCs and PtNCs have been widely employed in different fields, especially in sensing [24], bioimaging [25] and catalysis [26].

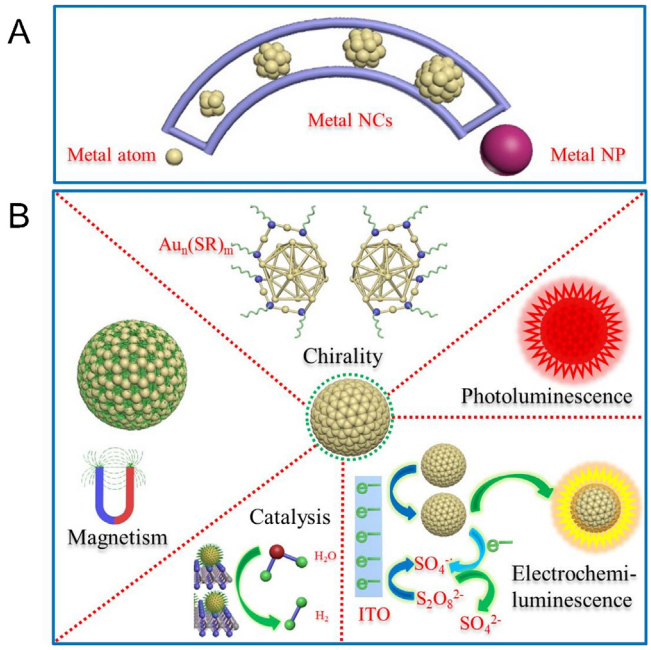

Fig. 1. Schematic illustration of (A) metal NCs bridging individual metal atoms and plasmonic metal NPs and (B) important properties of metal NCs related to their ultrasmall size. SR, thiolated ligand; ITO, indium tin oxide.

Despite swift progress in metal NC synthesis, most of the reported metal NCs suffer from poor stability against aggregation, limiting their use in many applications. For example, ultrasmall NCs may aggregate during a catalytic process, which can significantly reduce their catalytic activity. The immediate solution to this problem is to synthesize metal NCs that completely fulfil all requirements of the intended application. This strategy turns out to be rather challenging in practice because the large surface-to-volume ratio of metal NCs makes them intrinsically prone to react with the surrounding matter. An alternative strategy is to combine metal NCs with other nanoscale materials, forming metal NC-containing nanocomposites. Indeed, the combination of metal NCs with other nanoscale materials such as biomolecules, silica, metal-organic frameworks (MOFs) [27] and graphene [28], can remarkably enhance the properties of metal NCs. For example, the retrained dynamics of the NCs within nanocomposites often leads to improved stability and luminescence, whereas immobilization of metal NCs on graphene can improve their catalytic activity due to efficient electron transfer and good reactant transport in the composite [28]. Nanocomposites can also perform multiple functions in a single entity, which cannot be furnished by metal NCs alone [29]. For example, conjugation of metal NCs with other luminescent probes enables robust luminescence sensing in a ratiometric manner [30]. To exploit this potential, huge research efforts have been devoted to the development of various functional metal NC-based nanocomposites, and impressive progress has been made over the past decade.

Many excellent reviews have appeared in recent years, covering the synthesis, properties and applications of metal NCs [26,31–34]. Realizing that a review specifically addressing the development of metal NC-based nanocomposites has not yet been published, we have aimed to systematically compile recent research on metal NC-based nanocomposites in this work, focusing primarily on their synthesis, function and application. We begin with a brief introduction of several distinct properties of metal NCs, followed by an overview of strategies to synthesize nanocomposites including metal NCs from different materials. We then highlight important and representative applications, focusing on the areas of sensing, imaging and catalysis. Finally, we express our views on existing challenges and future developments in the field.

Distinct properties of metal NCs

The key characteristic of metal NCs is the small number of atoms in their cores. The resulting ultrasmall size (diameter < 2 nm) is comparable to the Fermi wavelength of electrons, resulting in the breakup of the band structure of the bulk metal into discrete energy levels. As a result, metal NCs exhibit many intriguing prop-

erties that are significantly different from those of larger metal NPs. Unraveling the total (core plus surface) structures of metal NCs is of paramount importance for understanding their stability, metal-sulfur interfacial bonding and physicochemical properties. Especially single-crystal X-ray crystallography can capture NC structure with atom-level precision [35,36]. X-ray absorption spectroscopy (XAS) has also been employed for site-specific analysis of local structure and electronic character [37]. Furthermore, recent years have witnessed a rapid increase of electrospray ionization mass spectrometry (ESI-MS) applications in noble metal NC analysis [38,39], by which the composition (number of metal atoms, ligand molecules, and overall charge) can be determined for both pure noble metal NCs and alloy samples.

Systematic compilations of the properties of metal NCs can be found in excellent reviews [19,40]. In the following, we will restrict ourselves to those properties that are related to the application of metal NC-based composites in sensing, imaging and catalysis. One of the most fascinating features of metal NCs is their strong molecule-like photoluminescence. Although light emission can also be detected from bulk metals [41] and metal nanostructures [42,43], their luminescence quantum yield (QY) is only in the range of $10^{-10} - 10^{-5}$, too low for any practical application. In stark contrast, subnanometer metal NCs exhibit much enhanced luminescence, with a QY in the range of $10^{-3} - 10^{-1}$, which makes them well suitable for a wide range of luminescence-based applications. It is now well accepted that there are two different mechanisms responsible for photoluminescence of metal NCs [43]. Firstly, it can arise from intraband (sp-sp) transitions due to the inherent quantization effects of metal NCs, as reflected by their size-dependent emission wavelengths and nanosecond luminescence lifetimes. Secondly, photoluminescence may also result from metal-ligand charge transfer processes. In this case, the emission is strongly affected by the properties of the surface ligands, and exhibits lifetimes up to microseconds. Notably, in some metal NCs, luminescence can occur *via* both mechanisms [44]. Metal NCs also feature large Stokes shifts and a reasonable resistance against photobleaching. These photophysical properties together with their ultrasmall size and good biocompatibility make metal NCs attractive optical probes for luminescence-based sensing [45] and bioimaging [25]. Notably, their long luminescence lifetimes allow time-gated imaging and sensing, yielding a high signal-to-background ratio [46].

Metal NC nanocomposites often exhibit aggregation induced emission (AIE), a phenomenon first reported by Xie and coworkers in 2012 [47]. They observed that nonluminescent, oligomeric Au(I)-thiolate complexes displayed strong luminescence upon aggregation, with intensity and color modulated by the degree of aggregation. The AIE discovery was successfully harnessed to synthesize highly luminescent AuNCs [47]. Subsequently, researchers utilized the AIE effect to improve the stability and emission intensity of CuNCs by entrapping them in MOFs [48], resulting in a more than 20-fold increase of the photoluminescence QY (from 0.5%–11%), extended excited-state lifetime (from 1.3–11.1 μs) and improved photostability. Novel composite probes (SiNPs@GSH-AuNCs) with dual-color emission were developed by combining amino-modified silicon NPs (SiNPs) and glutathione (GSH) capped AuNCs (GSH-AuNCs) [49]. Transmission electron microscopy (TEM) and dynamic light scattering revealed self-assembly of large (diameter 0.2–1.2 μm) spherical particles mediated by electrostatic interactions, in which the SiNPs retained their blue emission at 450 nm, whereas AIE-enhanced luminescence of the GSH-AuNCs appeared at 570 nm. In another study, positively charged hypromellose grafted chitosan (HGC) was employed as a matrix to fabricate composite films by dehydration-triggered aggregation of negatively charged CuNCs [50]. The resulting HGC-CuNCs films were transparent and showed AIE-enhanced photoluminescence with a QY of 42%, presumably due to the restricted rovibrational dynamics of the CuNCs within the polymer network.

Metal NCs can also show interesting electrochemiluminescence (ECL) effects, resulting from interactions between electrochemically produced, highly reactive radical species [51]. In contrast to photoluminescence, ECL does not require light irradiation and thus avoids background arising from scattered excitation light. Therefore, ECL has long been recognized as a powerful analytical tool, particularly in the development of highly sensitive sensors [52]. ECL activity of metal NCs was first reported by Ras and coworkers [53] in 2009, when they observed that polymethacrylic acid-stabilized AgNCs exhibited cathodic, hot electron-induced ECL. Later on, other NCs including AuNCs [54,55] and CuNCs [56] were also reported to show strong ECL. Significant efforts have been focused on the analysis of metal NC-based ECL [57]. Mechanistic studies revealed that factors such as metal core size and charge as well as protecting ligands all have a significant effect on the ECL wavelength, intensity and efficiency [58].

Metal NCs exhibit interesting and peculiar behavior in their interactions with biological systems [59]. Owing to their extremely large surface-to-volume ratio, they are prone to interact with the surrounding biomaterials. As our own studies have revealed, proteins bind to metal NCs (*i.e.* Au and Ag NCs), causing significant changes of their photophysical properties [60,61]. Unlike the markedly larger NPs, which can adsorb many protein molecules, either as monolayers on smooth surfaces [62–66] or dispersed in polymeric brushes [67], ultrasmall NCs bind proteins roughly on a 1:1 basis or interact with only a subunit of a multi-domain protein [68]. Moreover, cellular uptake differs from that of larger NPs (diameter $\tilde{1}$00 nm). While large NPs are directly internalized by cells without prior accumulation at the plasma membrane [69], metal NCs adsorb onto the membrane before gradually appearing inside the cells [59,70]. Apparently, multiple NCs need to interact simultaneously with membrane receptors in close proximity to trigger the endocytosis machinery [59]. Furthermore, unlike larger NPs (diameter > 5 nm), which typically accumulate in the mononuclear phagocytic system (*e.g.*, liver or spleen) and cause long-term toxicity, the small size of metal NCs permits efficient clearance (*via* the kidneys) from the body [71]. This reduces toxic side effects, which is important for biomedical applications and especially in the clinical setting. Beyond the intrinsic properties of metal NCs, the coating ligands can also have a strong influence on their biological interactions [72].

Metal NCs, especially AuNCs, have also been recognized as a novel and promising type of catalyst. Compared with conventional metallic NP catalysts, metal NCs provide more active sites due to their higher percentage of exposed surface atoms and thus may exhibit enhanced or sometimes different catalytic properties [15]. Rapid advances in the synthesis strategies have made it possible to produce atomically precise metal NCs, greatly facilitating studies aimed at a mechanistic understanding of metal nanocatalysts, *e.g.*, the size dependence of the catalytic activity [73]. With atomically precise composition and structure, it is indeed possible to relate the structure of metal NCs to their catalytic properties. For example, for the catalytic performance of thiolate capped AuNCs for the selective oxidation of styrene by O_2, it was found that smaller AuNCs show higher catalytic activity than larger ones, whereas the selectivity was similar among differently sized NCs [15]. In addition, AuNCs can be doped with a single atom of another metal, allowing the catalytic properties to be tuned on an atom-by-atom basis [74]. Several recent studies have also examined the effects of ligands on the catalytic activity, accessibility, selectivity and stability of metal NC catalysts [40]. For example, Xie and coworkers [75] found that a shorter alkyl chain offers a better accessibility for substrates and a higher catalytic activity. Moreover, ligands can also control the

exposure of active sites on the surface of metal NCs and modulate the adsorption of substrates.

Synthesis approaches of metal NC-based nanocomposites

Different strategies can be adopted to synthesize metal NC-based nanocomposites, depending on the properties of the materials or the intended application. In general, metal NCs can be integrated into other materials in two different ways: post-synthesis functionalization (after synthesis) and *in-situ* functionalization (during synthesis). For the post-synthesis approach, there are various strategies, including chemical conjugation, non-covalent interactions, self-assembly and ligand exchange (Fig. 2). In the following, we give a detailed overview of these strategies.

Chemical conjugation

Chemical conjugation mainly relies on interactions between the terminal functional groups of metal NCs and groups on the complementary molecules/materials. One such conjugation method is N-(3-dimethylaminopropyl)-N-ethyl carbodiimide (EDC) activated amide bond formation between amine and carboxylic groups. As an example, bovine serum albumin (BSA)-stabilized AuNCs were first carboxylated by glutaraldehyde and glycine, and then conjugated with amino groups-bearing Herceptin monoclonal antibodies *via* EDC activation in the presence of NHS (*N*-hydroxysuccinimide, Fig. 3A) [76]. The successful conjugation was confirmed by the size increase upon forming Herceptin-AuNC composites. TEM images further revealed that the AuNC-Herceptin conjugates were uniformly distributed and no aggregates were present. As demonstrated by Wang et al. [48], both stability and luminescence of CuNCs can be significantly improved upon incorporation into zeolitic imidazolate frameworks-8 (ZIF-8) (Fig. 3B). In fact, the stability was extended from hours to weeks, and the photoluminescence QY was 20-fold enhanced. These nanocomposites were produced by mixing Zn^{2+} and CuNCs, followed by adding 2-methylimidazole (2MIm) to form ZIF-8 with simultaneous incorporation of CuNCs. Two-dimensional (2D) zirconium-based MOF nanosheets with embedded AuNCs could be produced by using a similar approach [77]. Recently, Gao et al. [27] reported a crystalline ion (Zn^{2+}) triggered growth strategy to fabricate highly luminescent AuNC@ZIF-8 nanocomposites. Water-dispersible AuNCs were first precipitated by Zn^{2+} and then encapsulated into ZIF-8 in methanol by mixing with a methanolic solution of zinc nitrate and 2MIm. Compared with plain AuNCs, the AuNC@ZIF-8 nanocomposites exhibited a greatly enhanced QY and a longer luminescence lifetime (attributed to AIE). A highly specific response to H_2S was observed for the resultant AuNC@ZIF-8 nanocomposites. This Zn^{2+}-triggered growth strategy was subsequently extended to other systems such as AgNC@ZIF-8 and AuNC@ZIF-67, indicating the general adaptability of this design protocol.

Silica coating of pre-synthesized metal NCs provides another effective strategy to fabricate multifunctional nanocomposites. Particularly, compared with plain metal NCs, metal NCs@SiO_2 composites can protect NCs from aggregation and allow easy surface functionalization with different kinds of biomolecules. There are several strategies to create metal NC-silica conjugates. One of the most popular strategies is *in-situ* growth of a silica shell on the surface of pre-synthesized metal NCs *via* the famous Stöber method. Notably, due to the small size of metal NCs, it is rather challenging to coat silica on their surfaces in a well-controlled manner [78]. Muhammed and Pradeep were the first to successfully encapsulate AuNCs within a silica layer [79]. As shown in Fig. 4A, they synthesized (3-mercaptopropyl)trisilanol-stabilized Au_{25}NCs (Au_{25}@MPS) by reaction of GSH-protected AuNCs (Au_mSG_n) with (3-mercaptopropyl)trimethoxysilane (MPTS). Subsequently, they grew a thin silica layer directly onto the AuNC surfaces by hydrolysis and condensation at basic pH to obtain Au_{25}@SiO_2. Luminescent AuNCs stabilized with BSA have also been loaded into 100-nm silica NPs using a modified Stöber method [80]. These NPs displayed a monodisperse size distribution and good stability over months, and maintained the luminescence properties of AuNCs, with emission in the NIR region and a large Stokes shift. Recently, Wu et al. [81] prepared Gd^{3+}-AuNC aggregates and encapsulated them in a silica shell by adding tetraethyl orthosilicate (TEOS, Fig. 4B). The Gd^{3+}-AuNC-silica composites had an average diameter of 80 nm with a small size dispersion (Fig. 4C). Their luminescence was significantly enhanced with respect to that of individual AuNCs, and the introduction of Gd^{3+} endowed them with MR imaging capability. Most often, metal NCs are placed inside the core of NC-silica nanocomposites. Interestingly, by taking advantage of hollow mesoporous silica shell structures, AuNCs can also be deposited inside the shells (Fig. 4D) [82], resulting in superior stability in the biological environment and, thereby, better applicability in bioimaging and therapy.

Electrostatic interactions

Exploiting non-covalent interactions such as electrostatics is also a good way to fabricate NC-based nanocomposites. For example, a nanocomposite can be assembled from GSH-protected AuNCs, which are negatively charged at neutral pH, and carbon dots synthesized from polyethyleneimine (PEI), which are positively charged. The close proximity of the two components gives rise to an enhanced luminescence of the AuNCs due to resonance energy transfer from the carbon dots [83].

As depicted in Fig. 5A, Duan and coworkers [84] introduced an elegant approach to generate AuNC-based ultrathin films (UTFs) by immobilizing AuNCs within layered double hydroxide (LDH) nanosheets, produced by layer-by-layer (LbL) deposition. In this procedure, electrostatic interactions between the positively charged LDH nanosheets and the AuNCs protected by negatively charged ligands are the main driving force to achieve the LbL assembly. Moreover, the positive charge on the LDH nanosheets significantly affects the configuration and valence state of the AuNCs, leading to more than fivefold enhancement of the AuNC luminescence QY. Similarly, by taking advantage of electrostatic interactions, Wang et al. [85] fabricated composite materials from AuNCs and magnetic iron oxide NPs for dual-mode (optical and MR) bioimaging, featuring good biocompatibility and water dispersity. Metal NCs have also been attached to the surface of pre-formed silica shells *via* electrostatic interactions in recent work by Lin et al. [86]. As shown in Fig. 5B, they prepared mesoporous silica-coated core-shell up-conversion NPs (UCNPs@MS) with amino functional groups, to which they attached negatively charged Au_{25}NCs to obtain UCNPs@MS-Au_{25} nanocomposites. Although this noncovalent approach is convenient and versatile, complications can arise from various factors that have to be carefully controlled during synthesis, including ionic strength, pH, and sign and magnitude of the charge.

Self-assembly

Molecular self-assembly has long been known to be a powerful approach to create novel multifunctional structures with good stability in sample ways [87]. Indeed, these self-assembly techniques often only require stoichiometric mixing of two components to form composites. However, non-covalently self-assembled nanocomposites are oftentimes only poorly stabilized and may fall

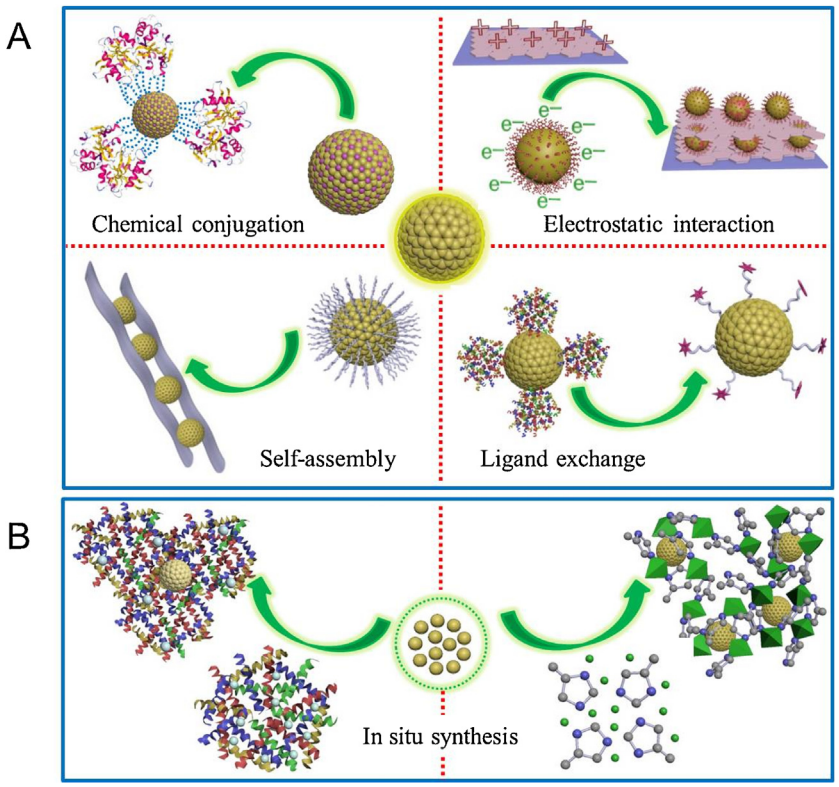

Fig. 2. Schematic illustration of two different strategies for fabricating metal NC-based nanocomposites. (A) Post-synthesis functionalization; (B) *in situ* fabrication during the synthesis of metal NCs.

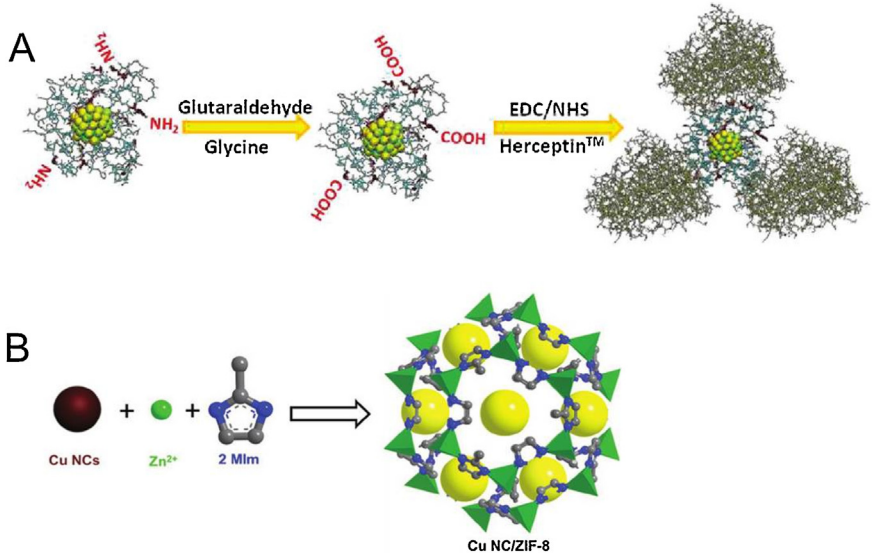

Fig. 3. Schematic depictions of two approaches for synthesizing metal NC-based composites by chemical conjugation. (A) EDC-activated linkage. (B) CuNC-ZIF-8 composites *via* direct formation of ZIF-8 in the presence of CuNCs. (Adapted with permissions from the American Chemical Society for (A), Ref. [76], and John Wiley and Sons for (B), Ref [48]).

apart in unfavorable environments offered by the intended applications. By using multidentate interactions, their stability can be greatly improved.

In recent work, Wang et al. [88] reported a simple strategy to fabricate fluorescent nanocomposites *via* self-assembly of AuNCs and polymers (Fig. 6A). AuNCs and poly(acrylic acid) (PAA) were modified with guest (adamantine, AD) and host (cyclodextrin, CD) molecules, respectively. The supramolecular interaction between host and guest components ensured formation of AuNC-polymer nanocomposites in a fast and simple way. Besides host-guest interactions, self-assembly can also be driven by electrostatic attraction. As recently reported by Bai et al. [89], well-organized, AuNC-incorporated nanogel structures can be obtained by self-assembly of negatively charged AuNCs and positively charged glycol-chitosan (GC) nanogel. The solution pH sensitively affects the formation of the self-assembled composite structures. Preparation at pH 6.0 was found to yield AuNCs@GC nanogels with the highest luminescence and excellent stability over the pH range

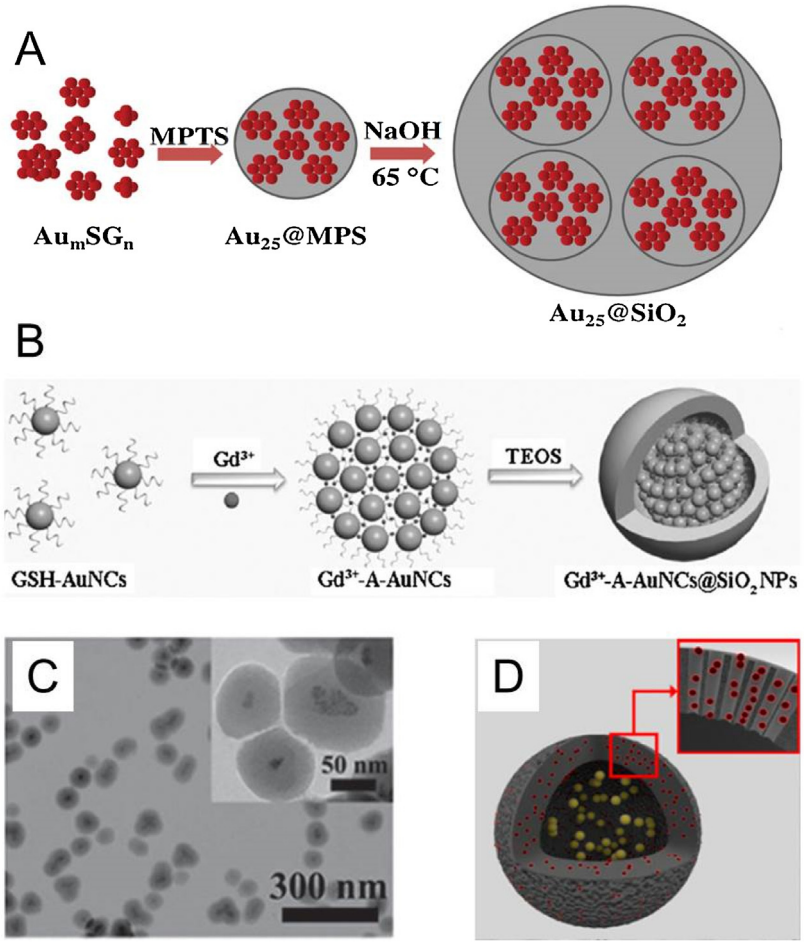

Fig. 4. Strategies for generating metal NC-silica nanocomposites. (A) Schematic illustration of the fabrication of Au_{25}@SiO_2 composites. (B) Illustration of the synthesis of Gd^{3+}-induced aggregates of AuNCs coated with silica; (C) high-resolution TEM images of the resultant Gd^{3+}-AuNC-silica composites. (D) Schematic of Au-silica composite spheres composed of hollow mesoporous silica shells hosting both AuNCs (red) in their mesopores and AuNPs (yellow) in their central cavity. (Adapted or reproduced with permissions from John Wiley and Sons for (A), Ref. [79], (B) and (C), Ref. [81], and the National Academy of Sciences for (D), Ref [82]).

0–14. Similarly, Guevel and coworkers synthesized self-assembled NPs based on electrostatic interactions between the cationic polymer poly(allylamine hydrochloride) (PAH) and AuNCs protected by GSH (Fig. 6B) [90]. Under optimized conditions NPs with low size dispersion and good colloidal stability were obtained, featuring pH-dependent swelling and shrinking as well as enhanced luminescence. Instead of cationic polymers, Cui and coworkers reported the use of Gd^{3+} to induce self-assembly of AuNCs into monodisperse spherical NPs [91]. The resulting nanocomposites showed enhanced luminescence, high X-ray attenuation and reasonable transverse relaxivity, making them promising as luminophores and contrast agents for optical, X-ray, and MR imaging, respectively. By taking advantage of the high affinity between gold and sulfur atoms, phosphine-protected AuNCs were attached to sulfur-functionalized graphene oxide (GO) *via* the displacement of one of altogether eight phosphine ligands decorating the AuNCs [92]. This approach provides a tight and robust attachment of metal NCs to graphene sheets.

Naturally occurring biopolymers such as proteins and DNA are known to self-organize into precisely defined functional structures [93], and certain peptides can self-assemble into nanostructures (*i.e.* nanofibers, nanotubes, vesicles) useful for biological applications [94]. Inspired by this natural process, Wang et al. [95] designed a multi-motif peptide which can generate luminescent peptide-protected AuNCs *via* a biomineralization process. Subsequently, the peptide-AuNCs undergo controlled supramolecular self-assembly into peptide nanofibers (Fig. 6C). Presumably, hydrophobic interactions are the key forces driving the peptide domains to organize into a fibrous structure. The luminescence of the AuNCs is nearly 70-fold enhanced in the composites. Considering the large chemical design variability and abundant functionalization capability of peptide building blocks, this strategy can easily be extended to other luminescent nanocomposites and more advanced functional materials.

Another widely used bioconjugation strategy is based on the strong yet noncovalent avidin-biotin bond. Pre-biotinylation of the AuNCs is necessary to bind the tetravalent avidin protein for conjugation with other components, for which a wide range of biotinylated conjugation reagents is commercially available. For example, AuNCs, prepared by controlled reduction of Au^{3+} in the presence of BSA, were first biotinylated at surface amino groups of BSA using biotin-N-hydroxysuccinimide ester, and then anchored to streptavidin-functionalized Fe_3O_4 NPs, resulting in multifunctional NPs for use in both MR imaging and NIR fluorescence molecular tomography [96]. Similarly, Au_{23}NCs synthesized with GSH were coupled to streptavidin *via* EDC, offering a wealth of further bioconjugation possibilities *via* biotin-avidin linkage [97]. We note that great care is advised to not excessively biotinylate the AuNCs, as this can lead to cross-linking and subsequent precipitation of AuNCs.

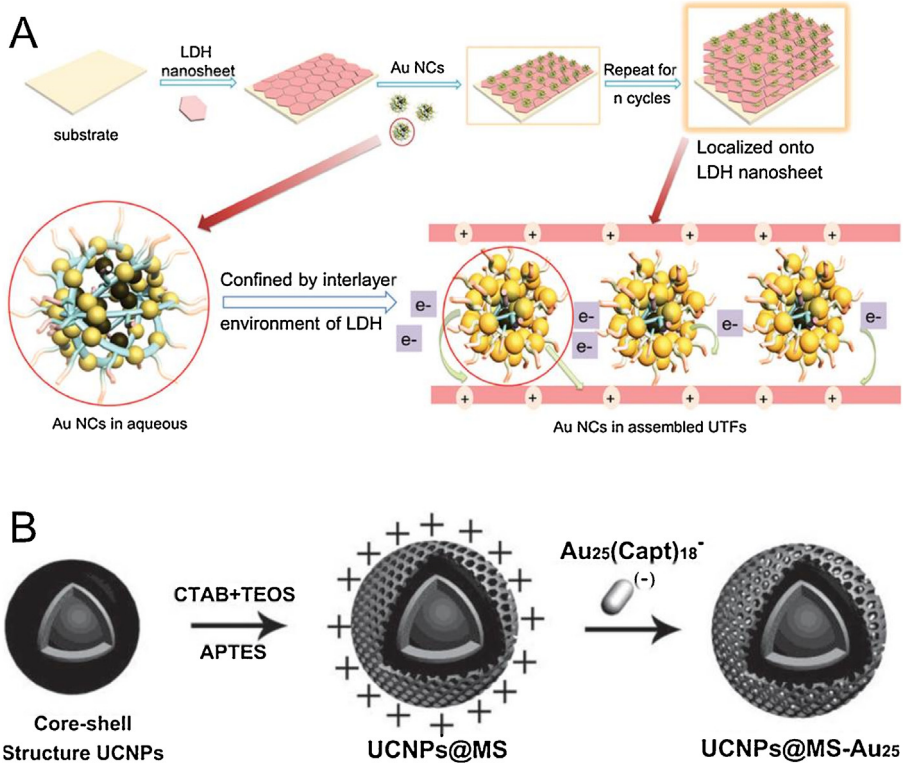

Fig. 5. Schematic illustration of preparing (A) multilayer films containing AuNCs and LDH nanosheets and (B) upconversion NP-AuNC composites *via* electrostatic interaction. (Reproduced with permissions from John Wiley and Sons for (A), Ref. [84], and (B), Ref [86]).

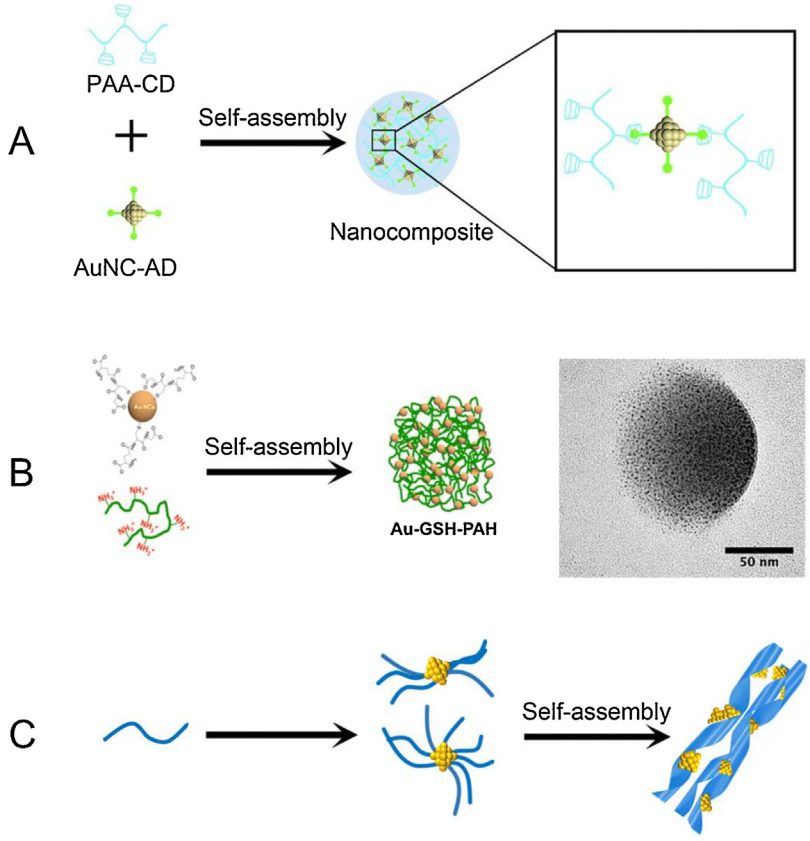

Fig. 6. Schemes for the synthesis of self-assembled AuNC-based composites *via* three different driving forces. (A) PAA-AuNC composites *via* host-guest interactions. (B) PAH-AuNC composites *via* electrostatic interactions. (C) peptide nanofiber-AuNC composites *via* hydrophobic interactions. (Adapted or reprinted with permissions from Elsevier for (A), Ref. [88], American Chemical Society for (B), Ref. [90], John Wiley and Sons for (C), Ref [95]).

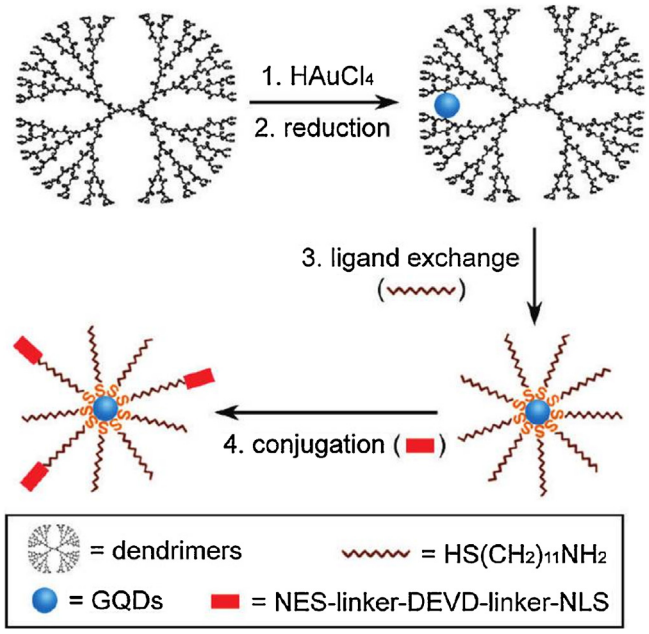

Fig. 7. Schematic representation of AuNCs (here denoted as gold quantum dots, GQDs) functionalized with a peptide moiety containing NES, caspase-3 recognition sequence DVED, and NLS *via* ligand exchange using MUA ($HS(CH_2)_{11}NH_2$). (Reprinted from Ref. [101] with permission from the American Chemical Society).

Ligand exchange

Ligand exchange is an alternative route for fabricating NC nanocomposites from pre-synthesized metal NCs. It involves mixing of NPs with free ligands that are capable of replacing the original ligands bound to the NP surfaces. Ligand exchange is a very important tool for preparing functional nanomaterials, especially metal NPs [98]. Early work by Hostetler et al. [99] already demonstrated ligand exchange as an efficient method to functionalize as-synthesized metal NCs with new ligands and additional functionalities. Particularly, ligands with specific bio-functions such as peptides are very promising for fabrication of multifunctional NC nanocomposites *via* ligand exchange. For example, Lo, Yang and coworkers [100] reported a novel strategy using 11-mercaptoundecanonic acid (MUA) as a ligand to extract AuNCs from encapsulation within polyamidoamine dendrimers. MUA does not only maintain the colloidal stability of the AuNCs in aqueous solvent, but also facilitates their further conjugation with various biomolecules. As an application, a peptide carrying a nuclear localization signal (NLS) sequence was anchored to the AuNCs, enabling their transport into the nucleus, as observed *via* their bright, localized photoluminescence.

Later, the same group adopted this ligand exchange strategy to functionalize AuNCs with a peptide moiety that contains both nuclear export signal (NES) and NLS sequences [101]. A caspase-3 recognition sequence, DEVD, was placed within the NLS/NES peptide to serve as a proteolysis site for the activated form of the apoptotic protease caspase-3 (Fig. 7). The NES-linker-DEVD-linker-NLS peptide enabled AuNCs to function as molecular probes for real-time monitoring of cellular apoptosis. Note that this ligand exchange approach is limited by the availability of systems with acceptable ligand exchange efficiency. Thus, compared with other post-modification strategies, ligand exchange is rarely employed to fabricate NC-based nanocomposites. For these post-synthesis strategies to succeed, it is always necessary to remove free metal NCs from the nanocomposites prior to their application, *e.g.*, by centrifugation or gel electrophoresis.

In-situ synthesis

Surface ligands play key roles in the synthesis of metal NPs. On the one hand, ligands can provide the required colloidal stability as well as limit the growth of NCs so as to avoid formation of large NPs. On the other hand, surface ligands are the basis for further conjugation of NCs with other functional components [102]. In most cases, the NC composites are fabricated from pre-synthesized metal NCs as we discussed above; however, it is also possible to generate functionalized NC composites during the synthesis of metal NCs. Specifically, when using certain ligands with additional functionalities, *e.g.*, biomolecules and polymers with particular physicochemical properties, the synthesis of metal NCs and their functionalization can be achieved in one step. Evidently, this strategy is much simpler and more convenient than post-synthesis functionalization.

Proteins have frequently been used as templates to synthesize nanomaterials, owing to their biocompatibility, abundant chemical groups and good availability [103]. They have also been employed as functional ligands for *in-situ* fabrication of NC-based composites, either in their natural form or with customized modifications. Xie et al. [104] were the first to report the synthesis of fluorescent protein-templated AuNCs using BSA as both reductant and stabilizer. Following up on this pioneering work, various metal (*i.e.* Au, Ag, Cu, AuAg alloy) NCs were synthesized with different proteins as functional ligands [105], and the bioactivity of the proteins was retained after synthesis in many cases. For example, insulin-protected AuNCs were reported to have a bioactivity similar to that of commercial insulin [106]. Thus, these AuNCs bind to their cognate receptor to enter cells, as observed by confocal microscopy, suggesting that the conformation of the insulin was only minimally perturbed, presumably thanks to the relatively mild reaction conditions and ultrasmall size of the AuNCs. Based on molecular dynamics simulation, Sun et al. [107] recently designed fluorescent nanocomposites with multiple AuNCs within an apo H-ferritin (HFt) nanocage. They featured good NIR imaging capability for live animals and also retained the kidney targeting function of HFt, as revealed by both luminescence imaging and inductively coupled plasma mass spectroscopy (ICP-MS).

Owing to the presence of abundant chemical groups on protein surfaces, one can also *in-situ* fabricate more advanced NC composites by integrating other functional units. Xu et al. [108] recently created a tri-modal (NIR luminescence/MR/CT) imaging agent by synthesizing, in a single step, NPs composed of AuNCs and gadolinium oxide using BSA (Fig. 8A). Obviously, this approach is much simpler than chemical conjugation of gadolinium oxide (Gd_2O_3) or other Gd^{3+}-based agents with pre-synthesized AuNCs [109,110]. In some cases, it is also possible to first modify the proteins with particular functions and then synthesize metal NCs using the modified proteins as template, which offers another interesting strategy to produce multifunctional NC-based nanocomposites. For example, Gd_2O_3 was first incorporated into BSA, which then acted as a scaffold for *in-situ* synthesis of AuNCs (Fig. 8B) [111]. BSA surrounding the Gd_2O_3-AuNCs assemblies was further loaded with a therapeutic agent, indocyanine green (ICG). The resulting Gd_2O_3-AuNCs-ICG nanocomposites possessed excellent tri-modal (NIR/MR/CT) in-vivo imaging properties and appeared promising for combined photodynamic and photothermal therapy.

Instead of proteins, short peptides can also be used for one-step synthesis of functionalized NC composites. Peptide sequences can be specifically designed; their abundant chemical groups allow the synthesis of NC-peptide composites with specific properties, *i.e.* targeting and drug carrying capabilities. Whereas naturally occurring, short peptides such as GSH have been frequently used to synthesize luminescent metal NCs, they mostly act as stabilizers rather than functional units. In contrast, rationally designed, longer

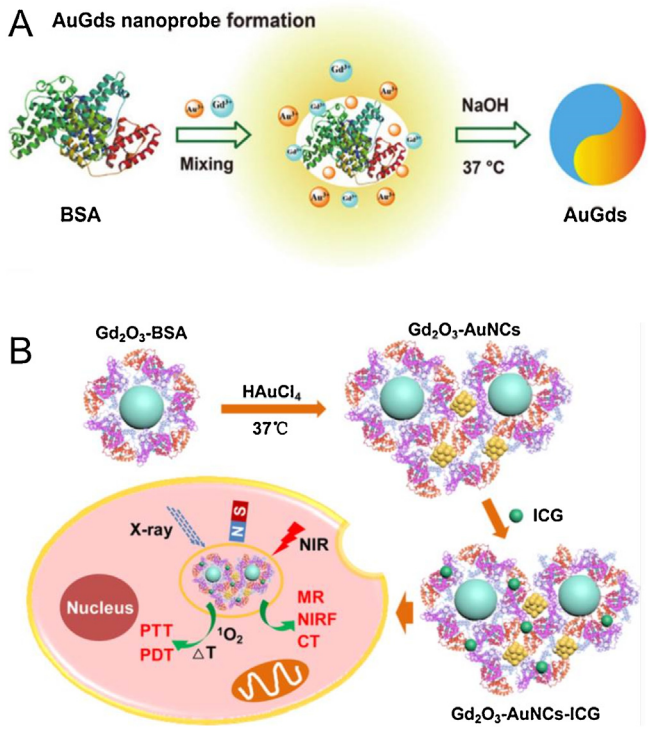

Fig. 8. Schematic illustration of the preparation of Gd-integrated AuNC composites templated with BSA. (A) Generation of AuGds from Au^{3+} and Gd^{3+} in the presence of BSA. (B) Pre-modification of BSA with Gd_2O_3, followed by AuNC formation and modification with ICG for multi-modal imaging. (Adapted with permissions from the Royal Society of Chemistry for (A), Ref. [108], and the American Chemical Society for (B), Ref [111]).

peptides have been employed for fabrication of NC composites with specifically designed properties [112]. In an early paper [113], Gao and coworkers reported a bifunctional peptide containing a domain capable of targeting the cell nucleus and a second domain capable of biomineralizing and stabilizing the AuNCs. The resulting peptide-conjugated AuNCs showed intense red emission and specifically targeted cell nuclei without any further modification. This strategy was later extended to peptide-conjugated CuNCs [114]. Huang and Liu [115] synthesized core–shell microspheres by *in situ* growth of PtNCs using GSH as a protective agent on the surface of PEI-modified Fe_3O_4. These nanocomposites were successfully applied to the detection of latent fingermarks in forensic science.

DNA oligonucleotides are another attractive type of ligand for functionalizing various nanomaterials, owing to their complementary base-paring, good biocompatibility and sequence design capability [116]. DNA binds metal cations and thus has been exploited as a template for synthesizing various luminescent Au, Ag, Cu and other metal NCs [117]. Particularly, the possibility to incorporate aptamers into the DNA sequence enables the synthesis of multifunctional DNA-metal NC composites within one step [118]. As an example, Zhu and coworkers [119] extended AS1411, a nucleolin-targeting DNA-aptameric anticancer drug, with poly(cytosine) *via* a pentathymidine loop and used it as a scaffold to synthesize AgNCs in a one-step process. The highly luminescent AS1411-AgNCs not only retained the anticancer functionality of the drug, but even exhibited a stronger growth inhibition compared with bare AS1411. Moreover, the AS1411-AgNCs were internalized by cells *via* receptor-mediated endocytosis and stained the nucleus. Most of these aptamer-AgNCs were prepared by using the natural dextro isomeric form of DNA (D-DNA) as a template, which is cleaved by nucleases prevalent in living matter [120]. The quenched emission and inhibition of the targeting function due to DNA digestion can severely hamper applications of natural DNA-templated AgNCs in biosensing and bioimaging. The enantiomeric form of D-DNA, levo DNA (L-DNA), displays a higher resistance to degradation than natural D-DNA and other modified nucleic acids [121]. Therefore, Feng and coworkers recently employed L-DNA instead of D-DNA to template the growth of AgNCs [122]. Their studies showed that L-DNA-templated AgNCs were indeed significantly more stable against nuclease digestion, thus making cell type-specific imaging at physiological temperatures possible with a much lower concentration of AgNC markers.

MOFs with well-defined and customizable pore structures are also promising templates for synthesizing nanomaterials with controllable size and dispersity [123]. It is fairly straightforward to incorporate different species such as metal NCs into MOF structures. Confinement of ultrasmall luminescent metal NCs inside MOF pores is expected to suppress non-radiative processes of metal NCs, leading to enhanced luminescence. In most approaches, pre-synthesized metal NCs are incorporated into the MOF structures during MOF formation. In an alternative strategy, AuNCs are generated directly inside the MOFs. The porous structures in MOFs limit both migration and aggregation of NPs, restrict NP growth and thus provide size control. In 2011, Jiang et al. [124] presented the first example of incorporating ultrasmall AuNCs in the pores of MOF structures by employing a predesigned hexagonal (4, 8)-connected MOF as the host. EXAFS spectra revealed the presence of ultrafine AuNCs with an average atom number of 2.5, corresponding to a mixture of Au_2 and Au_3 NCs. Later, atomically precise metal NCs inside MOFs were achieved by Liu et al. [125] through a simple, *in-situ* chemical reduction approach (Fig. 9). By elegantly controlling the reduction conditions, pure Au_{11}:PPh_3 NC@ZIF-8 and $Au_{13}Ag_{12}$:PPh_3@MIL-101 composites were obtained in a single step, showing that it is feasible to synthesize NC-MOF nanocomposites with exquisite size selectivity.

Application of metal NC-based nanocomposites

Many types of metal NC-based nanocomposites can be fabricated with the strategies discussed above. Often, the properties of metal NCs within the nanocomposites, such as the stability, luminescence properties and biocompatibility, are greatly improved with respect to bare metal NCs. Moreover, the presence of abundant surface functionalities and the possibility of conjugation with specifically designed motifs render these nanocomposites promising multifunctional platforms for a wide variety of applications. In this chapter, we will briefly review important advances made by using metal NC-based nanocomposites in sensing, bioimaging and catalysis.

Sensing

Luminescence sensing

Perhaps the most fascinating property of ultrasmall metal NCs is their molecule-like photoluminescence, which is preserved in most NC-based nanocomposites and endows them with great potential as luminescent probes in various analytical applications, particularly for sensing heavy metal ions, small biomolecules and biomacromolecules [126].

The detection of heavy metal ions in water and biological fluids is of paramount importance. Many different types of NC-based nanocomposites have been developed for heavy metal ion detection *via* their sensitive luminescence response. For example, Wang et al. [127] introduced a turn-on fluorescent sensor for Hg^{2+} detection based on carbon nanotube-AgNC composites (Fig. 10A). The luminescence of AgNCs stabilized by a thymidine-rich single stranded DNA (T-rich S1) is quenched when adsorbed onto the sur-

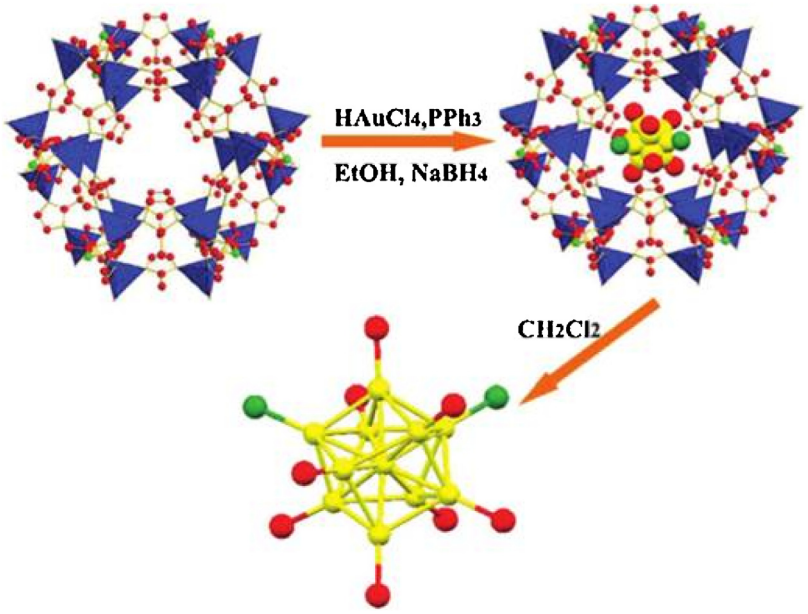

Fig. 9. Schematic illustration of synthesizing Au_{11} NCs inside the cavity of ZIF-8. PPh_3, triphenylphosphine. (Reprinted from Ref. [125], with permission from Royal Society of Chemistry).

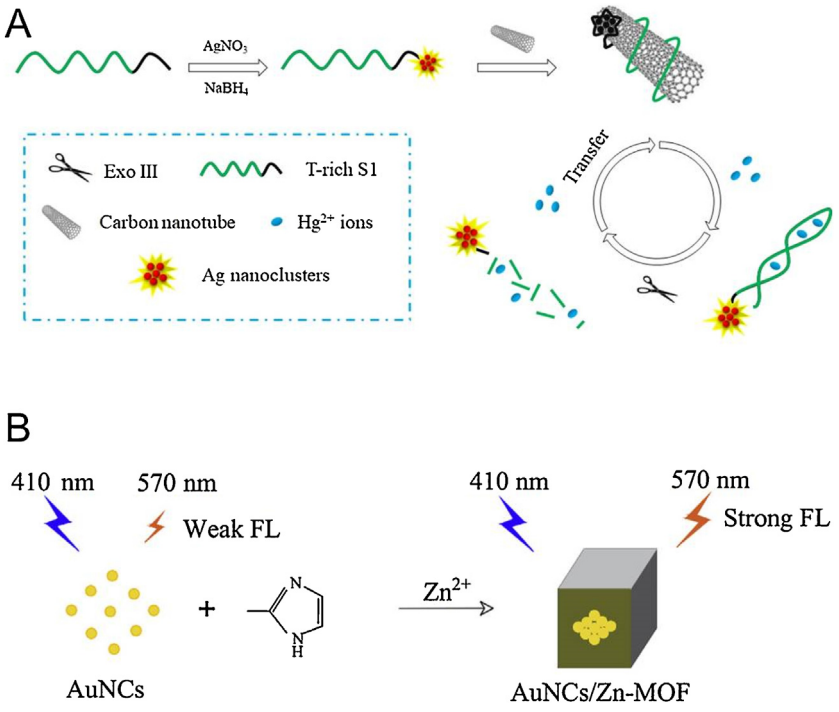

Fig. 10. Schematic illustration of sensing strategies for (A) Hg^{2+}, based on carbon nanotube-AgNC composites, and (B) Zn^{2+}, based on AuNC-MOF composites. FL, fluorescence. (Adapted with permissions from the Royal Society of Chemistry for (A), Ref. [127], Elsevier for (B), Ref. [128]).

face of a carbon nanotube due to energy transfer. In the presence of Hg^{2+}, interactions between the thymine bases and Hg^{2+} induces formation of a double-helical structure and releases the self-organized AgNCs-DNA conjugates from the carbon nanotubes. As a result, the photoluminescence from the AgNCs is restored, enabling the detection of Hg^{2+}. Using exonuclease III (Exo III) as a biocatalyst to cut the DNA, the bound Hg^{2+} ions are released. In this way, a highly sensitive luminescent sensing system based on carbon nanotube-AgNC composites was established, featuring a detection limit of 30 pM. Recently, Huang et al. [128] presented an interesting analytical application of AuNC-MOF composites for the sensitive detection of Zn^{2+} ions, which are essentially involved in a variety of biological processes (Fig. 10B). Their strategy is based on the AIE enhancement of GSH-capped AuNCs in aqueous solvent upon entrapment in a Zn-MOF, formed *in situ* in the presence of 2MIm and Zn^{2+}. Apart from Hg^{2+} and Zn^{2+}, photoluminescence detection of other metal ions such as Cu^{2+}, Pb^{2+}, Fe^{3+} and As^{3+} has also been reported with other metal NC-based composites [129–133].

The luminescence intensity depends on external parameters such as temperature, probe concentration and other experimental conditions, which requires careful calibration measurements to achieve high precision. Ratiometric sensing, which involves the

simultaneous detection of two luminescence signals at different wavelengths, is more robust and can yield a more reliable quantification due to cancellation of intensity-modulating effects [134]. Wang and coworkers [135] recently presented a ratiometric Hg^{2+} sensor based on dual-wavelength emission nanocomposites of carbon dots and AuNCs. The blue emission of carbon dots remained unchanged in the presence of Hg^{2+}, whereas the red emission from AuNCs gradually decreased upon successive addition of Hg^{2+}, resulting in a change of the emission color from pink to blue. Using a similar strategy, Wang et al. [136] loaded both AuNCs and carbon dots within hollow TiO_2 microspheres. Based on the distinctly different temperature responses of these two luminescent NPs, a dual-emission temperature sensor was established. With increasing temperature, the intensity of the red AuNC emission continuously decreased, whereas the blue carbon dot emission remained nearly constant, resulting in a continuous color change from red to purple that was easily observable by eye.

Highly porous materials such as MOFs are inherently sensitive for gas or vapor detection because they can concentrate analyte molecules to levels that are higher than in the external atmosphere [137]. In recent elegant work, Zang and collaborators [138] designed a light-emitting, porous MOF containing Ag(I) chalcogenide/chalcogenolate (SCC) clusters as building blocks. This SCC-MOF composite overcomes the poor chemical stability of typical AgNCs and exhibits remarkably enhanced luminescence upon proper control of the spatial separation and orientation of the NCs. The open channel structure of the MOF facilitates interactions of the AgNCs with external stimuli such as dioxygen (O_2) and volatile organic compounds (VOCs), resulting in fast luminescence turn-off by O_2 and turn-on by VOCs (*e.g.*, ethanol) in a highly sensitive manner (Fig. 11). This work vividly illustrates the great potential of designing functional metal NC-MOF composites for sensing applications. Indeed, Rogach and coworkers [48] recently showed that, even for CuNCs, which are less stable than AgNCs due to their stronger tendency to oxidize or aggregate, entrapment in MOFs can significantly enhance their QY and chemical stability. As a result, CuNC-MOF composites can be further developed into highly sensitive chemical sensors, *e.g.*, for trinitrotoluene detection.

In many applications, luminescent sensors experience harsh environmental conditions such as extreme acid/basic pH and high salinity, which challenge the stability of bare metal NCs. The use of nanocomposites can greatly help to solve this problem. For example, the AuNCs@GC nanogels developed by Bai et al. [89] exhibited excellent luminescence over the pH range of 0–14 and good salt tolerance, enabling the sensor to work robustly even under harsh conditions. As an alternative strategy, metal NCs can be coated with a silica layer, resulting in robust NC-silica nanocomposites with enhanced stability and dispersibility as well as good biocompatibility [139,140].

ECL sensing

Novel biosensors have been developed based on the ECL of metal NCs such as AuNCs [54]. In an early study, Zhu and coworkers [141] found that graphene-AuNC composites feature a higher ECL intensity than bare AuNCs. They exploited this composite to ECL emission-based, label-free detection of H_2O_2. The graphene component not only acts as a support for NC immobilization, but also serves as an ECL amplifier, greatly enhancing the sensitivity of detection. Based on the fact that phenolic compounds enhance the ECL signal at the graphene/multiwall carbon nanotube-AuNC composite-modified glassy carbon electrode in the presence of peroxydisulfate, an ECL sensor was fabricated for detection of phenolic compounds with high sensitivity, good repeatability and stability [142].

By combining TiO_2 nanoflowers as the co-reaction accelerator and dissolved O_2 as the intrinsic coreactant to generate the strong oxidizing intermediate radical $OH^{\bullet}$, AgNC-TiO_2 nanocomposites (Fig. 12A) were found to exhibit significantly enhanced ECL signals in comparison to bare AgNCs in solution [143]. Upon further introduction of ferrocene (Fc)-labeled DNA as an ECL quencher, a novel Fc-driven light switch biosensor was developed for ultrasensitive detection of amyloid-β (Aβ), as shown in Fig. 12. In this design, AgNC-TiO_2 nanocomposites are immobilized onto an electrode and exhibit a strong ECL signal (on-state). They function as sites for attachment of thiol-modified capture DNA (P_1). Subsequently, when Fc-labeled assistant DNA (P_2) hybridizes with P_1, the AgNC luminescence is strongly quenched due to the proximity of Fc (off-state). The overhanging part of P_2 hybridizes with secondary-target DNA (T), generated by an Aβ-induced immunoreaction based on DNA nanostructures. Thereby, Exo III cleavage is initiated, leading to the release of the Fc quencher from the AgNC-TiO_2 composites, and the ECL signal is switched on again. This assay for Aβ detection showed excellent sensitivity with a linear range from 50 fg/mL to 500 ng/mL and a limit of detection down to 32 fg/mL. While most reported ECL systems are based on the cathodic ECL emission of metal NCs [143–145], Yang et al. [146] recently reported an anodic ELC system of PtNC-graphene composites for detection of Cu^{2+}. Nanocomposites of AuNCs with graphene quantum dots (GQDs) were also found to exhibit stronger and more stable anodic ECL emission in comparison to AuNCs only and have been employed for constructing a pentoxifylline ECL sensor [147]. The enhanced ECL intensity and stability of the as-prepared Au NCs@GQDs were attributed to efficient resonance energy transfer between the GQDs and AuNCs acting as donors and acceptors, respectively, as well as the high electrical conductivity of the GQDs.

Colorimetric sensing

Colorimetric sensing is a simple method for detecting target analytes by monitoring the color change of a solution, featuring low cost and good portability. Whereas plasmonic metal NPs show strong absorption in the visible and have been widely adopted for colorimetric sensing [148], metal NCs are less suitable for colorimetric sensing due to the absence of the surface plasmon resonance effect. However, recent studies revealed high enzyme-like catalytic activity of some nanomaterials including metal NCs, opening up opportunities for developing NC-based colorimetric sensors [149].

In 2011, Wang et al. [150] were the first to report high peroxidase-like catalytic activity of BSA-AuNCs, based on which they developed a novel colorimetric assay for H_2O_2 with a detection limit of 20 nM. These composites catalyze the oxidation of a peroxidase substrate, 3,3′,5,5′-tetramethylbenzidine (TMB), by H_2O_2, yielding a blue-colored product with maximum absorbance at 652 nm. They also developed a simple yet highly sensitive colorimetric assay to detect xanthine, based on the production of H_2O_2 in the xanthine oxidase-catalyzed oxidation reaction. In contrast to natural enzymes such as horseradish peroxidase, BSA-AuNCs offer efficient enzyme-like catalysis over a wide range of temperatures ($4-90\,^{\circ}C$) and pH ($1-14$). Tao et al. [151] used GO to regulate the peroxidase-like activity of AuNCs and showed that GO-AuNC composites possess high catalytic activity over a broad pH range. They successfully employed folic acid-conjugated GO-AuNC composites as colorimetric probes for the detection of folate receptor (FR) overexpressing cancer cells such as HeLa and MCF-7. Exploiting the intrinsic peroxidase-like catalytic activity of AuNCs as well as the high loading and targeting ability of human epidermal growth factor receptor 2 (HER2) antibody-functionalized liposomes, AuNC-loaded, target-directed, functionalized liposomes were established as a robust sensing platform for amplified colorimetric detection of HER2-positive breast cancer cells with high sensitivity and selectivity (Fig. 13) [152]. Importantly, this method

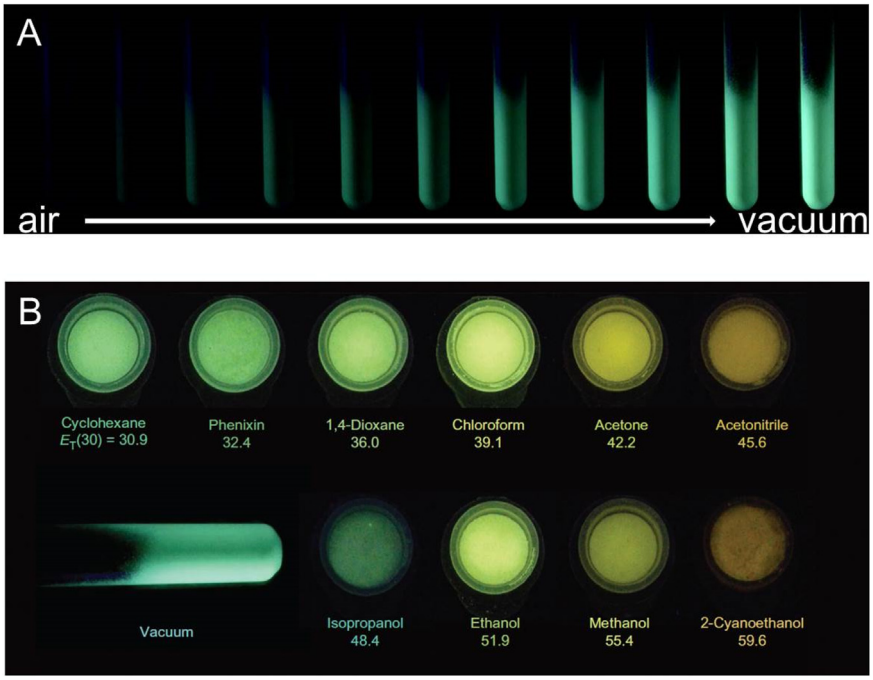

Fig. 11. Photographs of luminescent SCC-MOF composites excited by 365-nm light (A) inside a glass tube filled with air in the pressure range 0–1 at m. (B) Exposure of SCC-MOFs to VOCs with varying solvent polarity, $E_T(30)$. (Reprinted from Ref. [138], with permission from Nature Publishing Group).

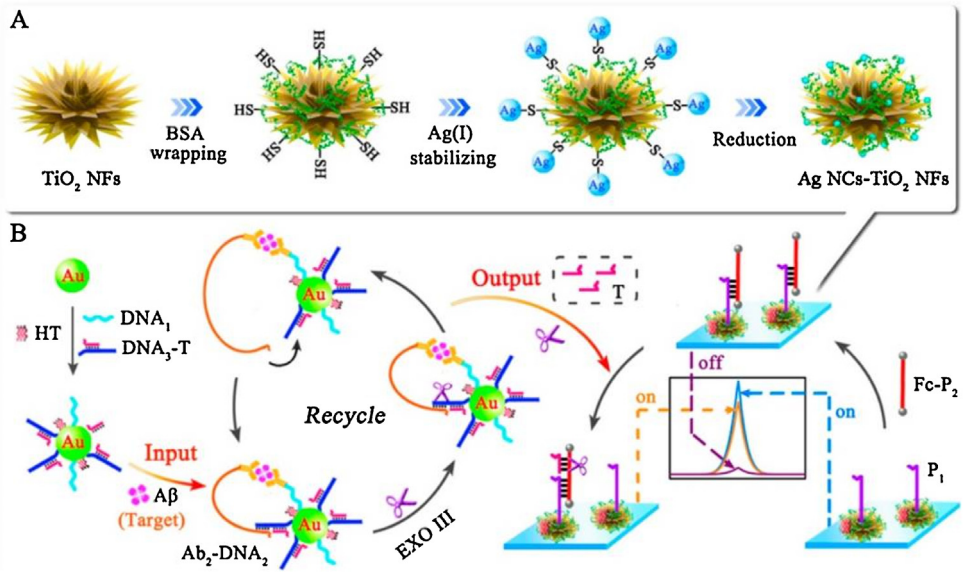

Fig. 12. Schematic diagrams showing (A) the preparation of AgNC-TiO_2 nanocomposites, and (B) the detection of Aβ by combining an immunoreaction-induced DNA nanostructure assembly with Fc-driven biodetection. (Reproduced from Ref. [143], with permission from the American Chemical Society).

was shown to be successful in detecting HER2-positive breast cancer cells in human serum samples as well as in breast cancer tissue.

To further enhance the enzyme-like activity of metal NCs and achieve better colorimetric sensing performance, Kim and coworkers recently proposed to combine AuNCs with another inorganic enzyme mimetics, Fe_3O_4 magnetic NPs (MNPs) [153]. The resultant AuNC-MNP composites indeed showed synergistic effects catalyzing the oxidation of TMB by H_2O_2, with about five times smaller apparent Michaelis-Menten constant, K_m, than the ones of AuNCs or MNPs alone. Furthermore, the AuNC-MNP composite-based sensing system can be used repeatedly *via* magnetic capture and washing steps.

Besides the widely studied AuNCs, composites of other metal NCs such as AgNCs [154], CuNCs [155], PtNCs [156] and alloy NCs [157] have also been employed in nanocomposites for colorimetric sensing, based on their catalytic properties. For example, DNA-templated AgPtNCs have been used as a colorimetric aptasensor for the detection of the target thrombin by virtue of their intrinsic peroxidase-mimicking activity [158]. To this end, the template DNA sequence for NC synthesis was fused with a thrombin-binding DNA aptamer, thereby avoiding an additional conjugation step of the AgPtNCs with the aptamer and preserving the affinity and specificity of the aptamer-NC composite to its target. This aptasensor was capable of detecting thrombin in complex biological fluids such as human serum with a detection limit of 2.6 nM.

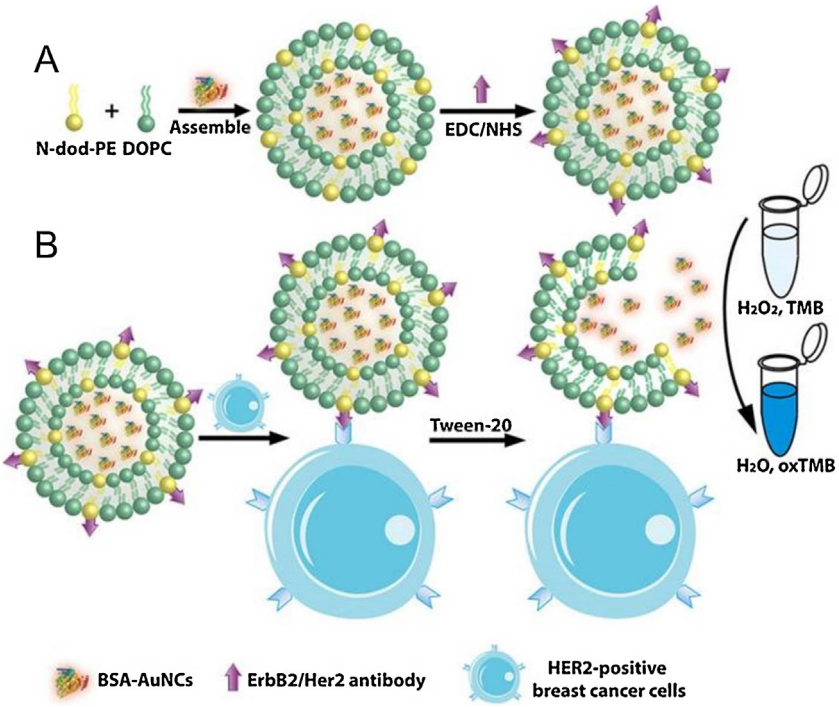

Fig. 13. Schematic depictions of (A) preparation of anti-HER2 conjugated liposome-AuNC composites and (B) HER2-positive breast cancer cell detection by using liposome-AuNCs-anti-HER2. (Reproduced from Ref. [152], with permission from Ivyspring).

Electrochemical sensing

Metal NCs are also well known for their high electrocatalytic efficiency, which has been harnessed for developing highly sensitive electrochemical sensors [159–161]. Zhang and coworkers [161] described microRNA (miRNA) detection *via* the electrocatalytic activity of oligonucleotide-encapsulated AgNCs. The high catalytic efficiency of AgNCs in response to H_2O_2 reduction resulted in a sensitive electrochemical miRNA biosensor without any laborious labeling and signal amplification, while the inherent selectivity of the molecular beacon probe endowed the biosensor with high base discrimination ability. Later, Wang and collaborators [162] reported another electrochemical miRNA sensor based on alkaline phosphatase (ALP)-incorporated AuNCs, with ALP catalyzing substrate dephosphorylation and AuNCs accelerating silver deposition. The signal amplification of ALP-AuNC-catalyzed silver deposition was monitored electrochemically, allowing ultrasensitive detection of free miRNAs in blood with a detection limit down to 21.5 aM as well as accurate identification of single-base mutants of the miRNAs.

Graphene is an ideal material for many electrochemistry applications because of its large surface area and excellent 2D electron conductivity [163]. Thus, combining metal NCs with graphene is expected to endow the NC composites with enhanced electrochemical properties and improved electrochemical sensing. In a recent study, AgNCs were loaded on GO to form AgNC-GO composites. GO was labeled with a detection antibody for electrochemical sensing of carcinoembryonic antigen (CEA), a tumor marker present in several cancer types (Fig. 14A) [164]. The catalytic activity of these AgNC-GO composites toward electrochemical reduction of H_2O_2 was significantly higher than the one of bare AgNCs owing to synergistic effects between AgNCs and GO. As a result, the assay showed a high sensitivity for CEA sensing with a detection limit of 0.037 pg/mL. Moreover, a sensitive electrochemical acetylcholinesterase biosensor based on AgNC-graphene composites was also developed and applied to the analysis of enzyme inhibitors [165]. Alternatively, AuNCs labeled with a cytosine-rich DNA probe were incorporated into graphene to electrochemically sense HIV DNA [166]. In combination with an Exo III-assisted target recycling amplification strategy, a detection limit for HIV DNA as low as 30 aM was achieved, which permits early detection of an HIV infection in human blood serum.

Besides graphene, other 2D materials have also been employed for fabricating composites with metal NCs for electrochemical sensing [167,168]. For example, Yang et al. [169] showed that a boron nitride-AuNC composite can be utilized as an electrochemical probe for immunosensing of interleukin-6 (Fig. 14B). Boron nitride (BN) sheets were exfoliated by using poly-diallyldimethylammonium chloride (PDDA) as a stabilizer and a linker, and then decorated with AuNCs *in situ via* an electrostatics-driven LbL assembly. The resultant PDDA-BN-AuNC composites were functionalized with antibody conjugates for use as luminescent or electrochemical markers for the detection of interleukin-6 in a sandwich bioaffinity immunoassay.

Bioimaging

In vitro *luminescence imaging*

Owing to the intrinsic luminescence and good biocompatibility of metal NCs, NC-based composites can be employed as robust optical probes in fluorescence imaging. To highlight specific molecules or cells, an imaging probe should have a high specificity for its target, which can be achieved by functionalization of pre-synthesized metal NC-based composites with a suitable targeting unit [170]. For example, folic acid-conjugated NC composites have been widely adopted for targeted imaging of FR-overexpressing cancer cells [171–173]. Furthermore, a label-free "turn-on" luminescence sensor for the detection of FRs was developed, based on resonance energy transfer between single-walled carbon nanotubes and AgNCs [174]. Kong et al. [175] reported a multifunctional nanoprobe for simultaneous targeting and imaging of human colon carcinoma Caco-2 cells by conjugating vitamin B12 to ribonuclease A–stabilized AuNCs. Triphenylphosphonium (TPP)

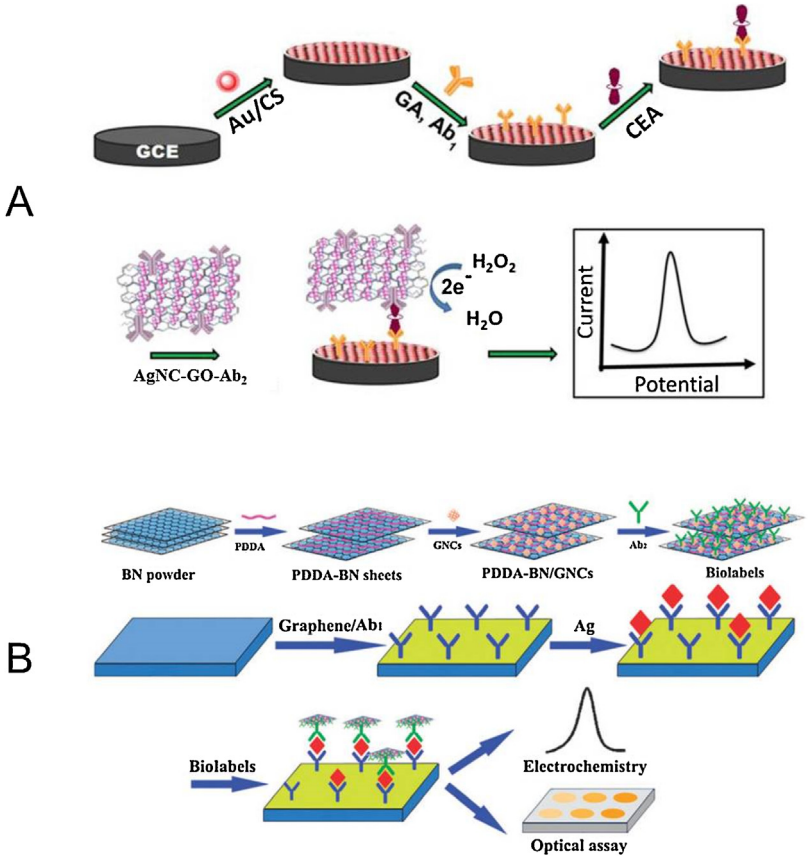

Fig. 14. Schematic diagram of the fabrication and electrochemical sensing mechanisms of (A) AgNC-GO composites for CEA detection. Top: Preparation of the electrode (GCE, glassy carbon electrode; Au-CS, chitosan-modified AuNP solution; GA glutaraldehyde, Ab_1, CEA capture antibody). Bottom: Binding of AgNC-GO composites to the electrode *via* detection antibody Ab_2. (B) PDDA-BN-AuNC composites for interleukin-6 detection. (Reproduced with permissions from Elsevier for (A), Ref. [164], Royal Society of Chemistry for (B), Ref. [169]).

is a delocalized lipophilic cation, which easily passes through phospholipid bilayers and accumulates in the mitochondria of living cells. TPP-functionalized chitosan-AuNC composites (AuNCs@CS) exploit these properties for imaging mitochondria within live cells [176]. Recently, by combining biomineralization and supramolecular self-assembly of motif-designed peptide constructs containing an RGD sequence, we have demonstrated the utility of AuNC-incorporated peptide nanofibers for targeted imaging of cancer cells [95].

Protein-metal NC composites can be directly utilized to selectively mark cells specifically recognized by the proteins. For example, Tf-AuNCs exhibit a high affinity to A549 lung tumor cells, which overexpress Tf receptors on their plasma membranes, as confirmed by cellular imaging [177], and Tf-functionalized CuNCs have also been used for imaging Tf receptor-overexpressing cancer cells [178]. Gao and coworkers reported that AuNCs templated with a bifunctional hexapeptide (CCYTAT) could specifically target the nuclei of human gastric mucosa cells (GES-1), human embryonic lung fibroblast cells (MRC-5) and HeLa cells [113].

Taking advantage of their good cellular imaging properties, metal NC-based composites have been developed for real-time imaging of important physiological events in the intracellular environment. For instance, a novel NC-based composite was fabricated through a crown-like assembly of dye-encapsulated silica particles decorated with satellite AuNCs for imaging highly reactive oxygen species (hROS) in live cells [179]. This composite exhibits single-wavelength excitation and dual-wavelength emission, at 565 nm from the AuNCs, which is markedly quenched in the presence of hROS, and at 435 nm from the silica particles providing an internal reference (Fig. 15A). Such a combination of selective photoluminescence quenching of the AuNCs with the high biocompatibility and stability against photobleaching of the silica NPs offers considerable advantages for monitoring intracellular signaling events. When the NC composite-loaded cells were incubated with H_2O_2, the strong emission in both blue and red channels remained constant (Fig. 15B). Upon incubation with 200 μM HClO for 5 min, however, the red emission almost disappeared, whereas the blue emission was still retained. Similar results were observed in the presence of 3-morpholinosydnon-imine (SIN-1) which slowly releases $ONOO^-$, another common hROS. Chen et al. [180] reported the use of BSA-templated cerium (Ce)AuNCs for monitoring the local pH inside cells. Their BSA-CeAuNCs exhibit dual emission at 410 nm and 650 nm, which is assigned to BSA-Ce complexes and BSA-AuNCs, respectively. The emission intensity of BSA-Ce complexes at 410 nm is highly pH-dependent, whereas the one of BSA-AuNCs at 650 nm is pH-independent. Local pH variations inside cells were observed with these nanocomposites by using ratiometric analysis.

In vivo *luminescence imaging*

The high luminescence and stability of NC-based composites make them especially attractive for *in vivo* imaging applications. Lee and coworkers recently showed that GSH-stabilized AuNCs exhibit significantly enhanced luminescence with a QY of up to 42% upon further conjugation with folic acid, which results from the rigidifying effect on the gold shell (Fig. 16A) [181]. As a result, a mouse injected with folic acid-AuNC composites showed extremely bright luminescence, with an average intensity more than 12-fold higher than the one observed for a mouse injected with only AuNCs

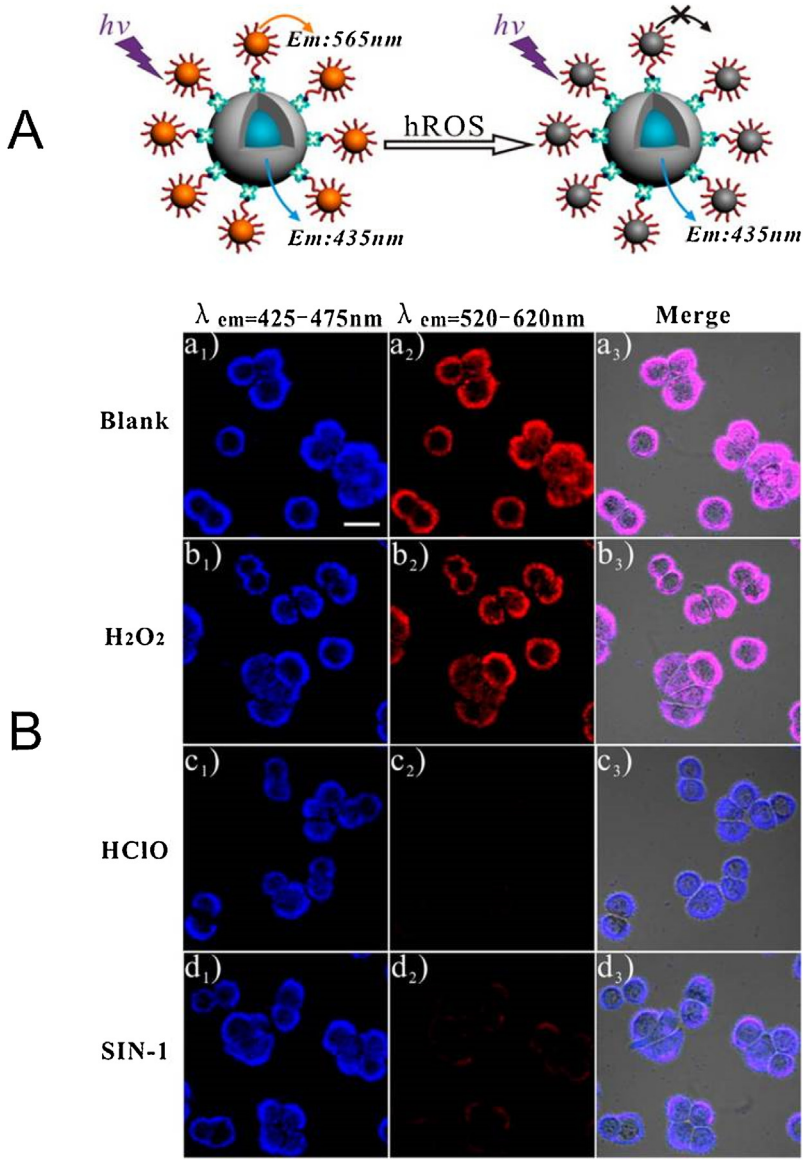

Fig. 15. (A) Schematic illustration of hROS detection using dye-encapsulated silica particles decorated with satellite AuNCs. (B) Confocal fluorescence microscopy images of HeLa cells after incubation with silica-AuNC composites for 1 h. Cells were (a) untreated or treated with (b) 1 mM H_2O_2 for 10 min, (c) 200 μM HClO for 5 min, and (d) 3 mM SIN-1 for 40 min. (Reproduced from Ref. [179], with permission from the American Chemical Society).

at the same dose (Fig. 16B). Unlike AuNPs larger than 10 nm [71], more than 90% of folic acid-AuNC composites were excreted *via* renal clearance within 24 h post injection.

In addition to brightness and stability, emission in the NIR is another desirable property of luminescent markers for in-vivo imaging because biological tissues show only weak absorption/scattering and autofluorescence in the NIR spectral window. NIR-emitting metal NC-based composites are promising for *in vivo* imaging [25]. In early work, Wu et al. [182] reported the first example of tumor imaging with NIR-emitting BSA-AuNCs. *In-vivo* tumor targeting and *ex-vivo* imaging studies showed that these NCs accumulated to a high level in tumor regions. Later, transferrin-functionalized AuNCs (Tf-AuNCs)-GO composites were fabricated and used as turn-on NIR fluorescence probes for imaging cells and small animals [183]. The presence of GO within the composites markedly quenches the NIR emission of Tf-AuNCs due to resonance energy transfer, which is, however, restored in the presence of Tf receptors. This composite enabled specific imaging of Tf receptor over-expressing HeLa cells of HeLa tumor-bearing mice. Recently, chitosan-stabilized, self-assembled AuNCs with a characteristic peak emission wavelength of 680 nm were also developed, and their utility for both *in-vitro* and *ex-vivo* cellular imaging has been investigated [184]. Interestingly, the fluorescence from the kidneys gradually increased over 6 h and then decreased again. These nanocomposites were renally excreted due to their ultrasmall dimensions, avoiding toxicity effects due to nonspecific accumulation in healthy tissues and organs.

In vivo *multimodal imaging*

Multimodal imaging, *i.e.*, the combination of two or more imaging modalities providing complementary information, offers distinct advantages. Accordingly, the development of multimodal imaging probes based on metal NCs for *in-vivo* imaging has attracted great attention in recent years. For dual-modality fluorescence/CT imaging of thyroid cancer, iodinated BSA-AuNC composites were fabricated by reaction of BSA-AuNCs with iodide ions *via* the oxidation of chloramine-T (Fig. 17) [185]. These composites were found to rival the clinical CT contrast medium, and

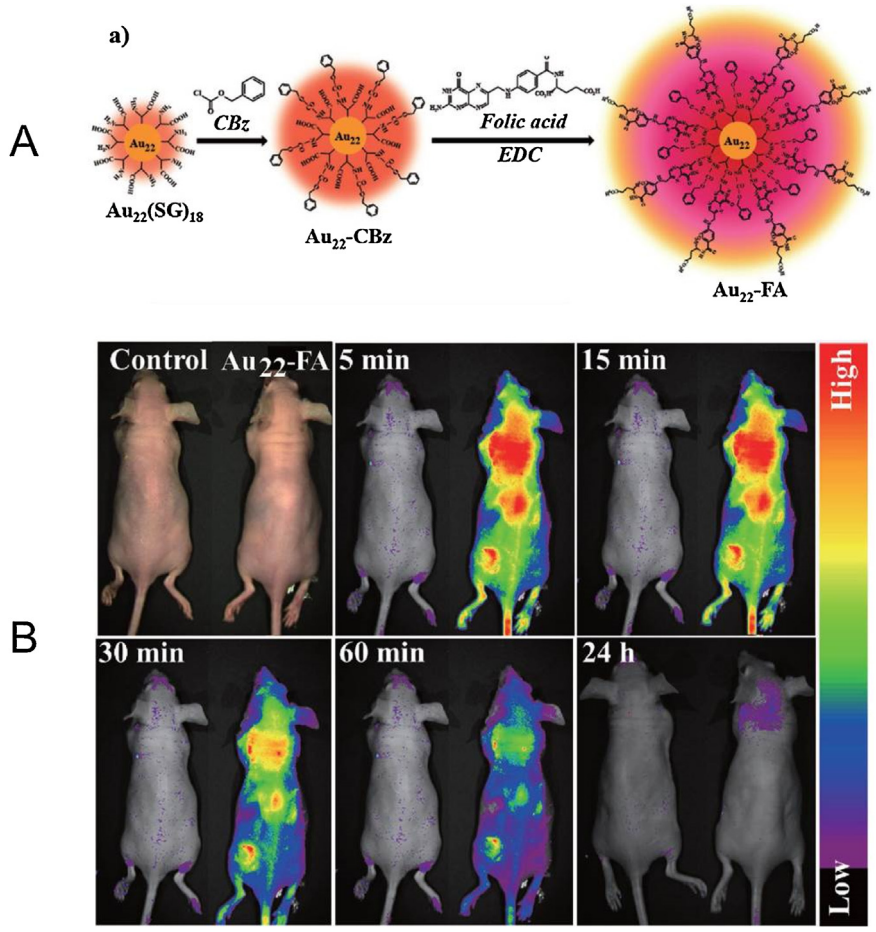

Fig. 16. (A) Synthetic scheme depicting the synthesis of folic acid-AuNC composites (Au_{22}-FA) from $Au_{22}(SG)_{18}$. SG, GSH conjugated to gold *via* thiolate bonding; Cbz, benzyl carbonochloridate. (B) Representative in-vivo luminescence images of control and IV-injected mice, collected at 5, 15, 30, 60 min and 24 h post injection. (Adapted or reproduced from Ref. [181], with permission from John Wiley and Sons).

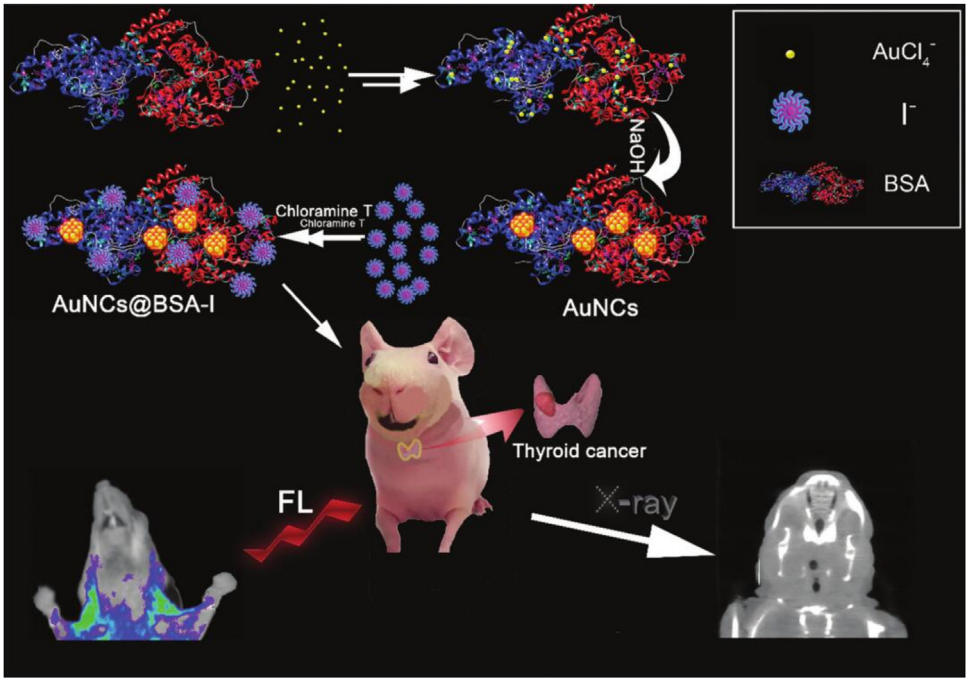

Fig. 17. Schematic illustration of the preparation of iodinated BSA-AuNC composites (AuNCs@BSA-I) for *in-vivo* dual-modality (fluorescence and CT) imaging. (Reproduced from Ref. [185], with permission from the Royal Society of Chemistry).

their luminescence emission spectrum falls in the NIR region. Both *in vivo* fluorescence and CT imaging of a human thyroid cancer tissue-derived xenograft model showed that these iodinated BSA-AuNCs were capable of accurately and selectively reveal thyroid cancer. Whereas iodine-based agents are effective in absorbing X-rays, they have only a short circulation lifetime, and non-specific distribution and potential renal toxicity have limited their application. Gold has a higher X-ray absorption coefficient than iodine, and shows approximately 2.7 times higher contrast per unit mass [186]. Therefore, the strong X-ray attenuation of AuNCs makes them a good alternative for multimodal imaging. For example, folic acid-conjugated GSH-capped AuNCs were employed for fluorescence/CT imaging of gastric cancer [187], and lysozyme-stabilized AuNCs were used for NIR fluorescence/CT imaging of tumor-bearing mice [188].

Compared with CT imaging, MR imaging has lower spatial resolution but higher sensitivity to soft tissues. Thus, combining MR with optical imaging has also been exploited to improve tissue imaging [189]. It is rather straightforward to achieve luminescence/MR dual-modality imaging by conjugating metal NCs with magnetic agents such as Gd-based compounds and iron oxide NPs. Gd^{3+} ions are excellent as contrast agent for MR imaging, and Gd^{3+}-chelates are extensively employed in clinics [190]. Liang et al. [110] designed a cyclodecapeptide that simultaneously generates AuNCs and coordinates with Gd^{3+} ions. Compared with Gd^{3+} chelates, gadolinium oxide (Gd_2O_3) NCs were reported to exhibit a larger proton relaxivity, which makes them promising as MR imaging agent [191]. BSA-templated Gd_2O_3-AuNC composites were synthesized *via* a biomineralization strategy for *in-vivo* NIR fluorescence/MR blood pool imaging [192]. Further conjugation with the RGD peptide rendered these Gd_2O_3-AuNC composites applicable to targeted tumor imaging in U87-MG tumor-bearing mice. Iron oxide NPs also hold great potential for MR imaging due to their high magnetization. Iron oxide NPs can easily be hybridized with metal NCs *via* different chemical conjugation approaches, including EDC coupling [193], electrostatic attraction [85] and biotin-streptavidin interactions [96].

Whereas optical, CT and MR imaging modalities all have their individual strengths and weaknesses, combining all three modalities within one probe can help to advance traditional diagnosis to accurately identify disease sites [194]. For example, AuNCs have been assembled into monodisperse spherical particles for tumor multimodality imaging by selectively inducing electrostatic interactions between Gd^{3+} and negatively-charged AuNCs (Fig. 18) [91]. The resulting Gd-AuNC composites possessed a good biocompatibility both *in vitro* and *in vivo*, and were well internalized by A549 cells. These composites were then employed as a multifunctional nanoplatform for optical/CT/MR imaging of xenografted A549 tumor models *in vivo*. Similarly, BSA-templated AuNC-Gd_2O_3 composites [108] and silica-encapsulated Gd^{3+}-AuNCs [81] have been synthesized and applied to tri-modal imaging of tumor-bearing mice. Hembury et al. [82] recently designed another novel tri-modal imaging probe, Au-Silica quantum rattles, composed of AuNCs within a mesoporous silica shell and AuNPs within the shell's central cavity. This design stabilizes AuNCs and preserves their optical activity and paramagnetism in the biological environment, so that they can serve as markers for multimodal (luminescence, photoacoustic and MR) imaging of LS174 T tumor-bearing mice.

Catalysis

Owing to their unique electronic structure and high fraction of surface atoms with low coordination numbers, metal NCs are typically more reactive, and can have improved and/or different catalytic properties in comparison to their NP counterparts. A large number of studies have demonstrated the good performance of metal NCs, especially AuNCs, in catalyzing various chemical reactions including oxidation, hydrogenation, coupling as well as electrocatalytical reactions [40]. During catalysis, these tiny clusters have to be protected from aggregation, *e.g.*, by introducing stable capping agents or distributing them on solid supports. Owing to the confinement effect and their crystalline pore structure, MOFs have been elegantly employed as solid supports for catalysis with metal NCs [195–197]. For example, AuNCs immobilized on MOF-199, synthesized by a one-step microwave irradiation strategy, exhibited high turnover numbers and frequencies in a three-component coupling reaction [198]. Owing to the confinement effect of MOF-199, the MOF-AuNC catalysts could be recycled five times without serious loss of activity and significant AuNC aggregation. Doping with other metal ions can modulate the electronic structure of the encapsulated NCs and further improve their catalytic activity. As a recent example, Cu doping of ZIF-8 nanorod arrays (NRAs) with encapsulated AuNCs (AuNCs@ZIF-8(Cu) NRAs) enhanced the interfacial catalytic efficiency [199], resulting in almost complete (98%) conversion of 4-nitrophenol (4-NP) into 4-aminophenol within 6 min. More importantly, the morphology, structure and catalytic activity of the AuNCs@ZIF-8(Cu) NRAs showed negligible changes even after 10 successive cycles, attesting to the superior stability of this robust three-dimensional, self-supported catalyst. Both the excellent catalytic performance and the stability of the AuNCs@ZIF-8(Cu) NRAs were attributed to synergistic effects between ZIF-8(Cu) and AuNCs. The organic linkers of ZIF-8 facilitate adsorption of π-electron rich 4-NP molecules for π-π stacking interactions. The Cu doping of the ZIF-8 framework modifies the surface electronic structure of the AuNCs, which markedly accelerates the formation of gold hydride intermediates. Moreover, the confinement by the porous ZIF-8 framework makes the AuNC active sites more stable and well accessible to substrates and also prevents agglomeration. Furthermore, this composite also features superior catalytic activity for other nitrobenzene compounds, such as 3-nitrophenol, 2-nitrophenol and *p*-nitroaniline.

Recent years have witnessed major breakthroughs in preparing atomically precise metal NCs, providing new opportunities to investigate atomic scale-precise, size-dependent catalytic properties and to obtain structural insight into catalytic mechanisms [26]. In 2016, Zhu and coworkers reported the first example of size-controlled growth of atomically precise metal NCs inside MOFs [125]. They discovered that Au_{11}NCs can be exclusively generated inside the framework of ZIF-8 and $Au_{13}Ag_{12}$NCs can also be *in-situ* prepared in MIL-101. Moreover, these highly dispersed metal NC@MOF composites exhibit remarkable stability and high catalytic activity in the oxidation of benzyl alcohol (Fig. 19A). This elegant work provides a new method for the size-confining growth of atomically precise AuNCs in MOFs for heterogeneous catalysis. Later, the same group established another approach based on electrostatic attraction to controllably encapsulate atomically precise NCs into MOF structures [200]. This strategy proved to be capable of synthesizing various atomically precise metal NC-MOF composite catalysts, including all combinations of $Au_{12}Ag_{13}$, Ag_{44} and $Ag_{12}Cu_{28}$ NCs with ZIF-8, ZIF-67 and manganese hexacyanoferrate hydrate frameworks. Moreover, $Au_{12}Ag_{32}$-ZIF-8 composites showed excellent performance in capturing CO_2 and converting phenylacetylene into phenylpropiolate under mild conditions with a high turn-over number, far exceeding those of most known catalysts (Fig. 19B). It is believed that these atomically precise metal NCs@MOF composites will be of great help to understand the mechanisms of nanocatalyst surface reactions and open new opportunities in heterogeneous catalysis. This issue is nicely illustrated in recent work of Xie and coworkers [201], who studied the Au_{25}NC-catalyzed 4-NP hydrogenation by $NaBH_4$ to exam-

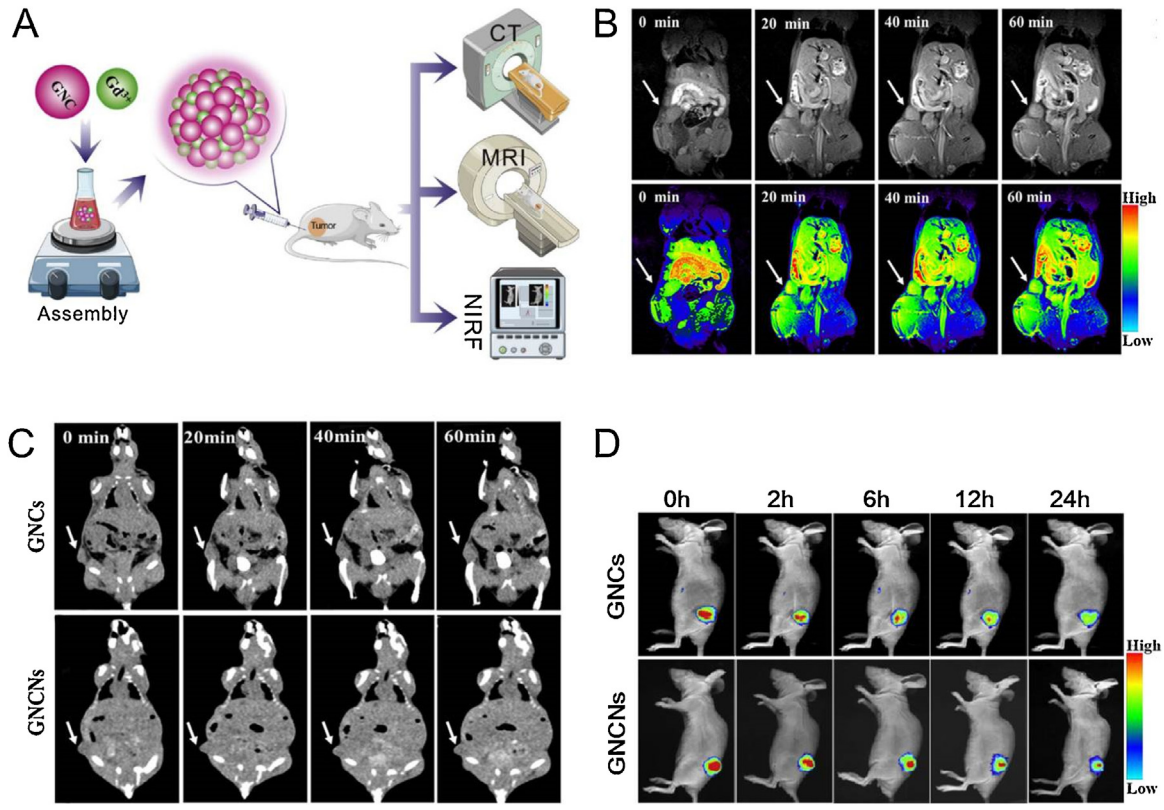

Fig. 18. (A) Schematic illustration of the preparation of Gd-AuNC composites for *in vivo* tri-modal cancer diagnosis. (B) *In vivo* T_1-weighted MR images upon injection of Gd-AuNC, (C) CT and (D) luminescence images of A549 tumor-bearing mice marked by intravenous injection of Gd-AuNC composites or AuNCs at different time points. (Adapted from Ref. [91] with permission from Elsevier).

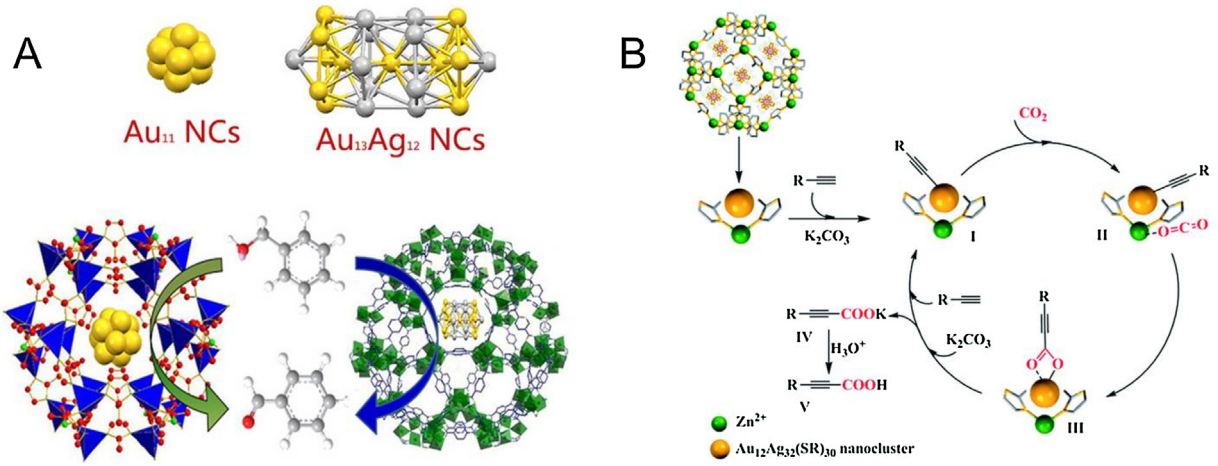

Fig. 19. Schematic illustration of (A) Au_{11}NC-ZIF-8 and $Au_{13}Ag_{12}$NC-MIL-101 composites for catalyzing the oxidation of benzyl alcohol; (B) $Au_{12}Ag_{32}$NC-ZIF-8 composites for capturing CO_2 and converting phenylacetylene into phenylpropiolate. (Reproduced with permissions from the Royal Society of Chemistry for (A), Ref. [125], and (B), Ref [200]).

ine the effect of protective ligands on the catalytic performance. They showed that a well-defined ligand (mercaptobenzoic acid) shell not only endows the Au_{25}NCs with good colloidal stability in solution, but also provides a unique environment for activating a specific reaction pathway involving adsorption of two 4-NP molecules, formation of a 4,4′-dihydroxyazobenzene intermediate, and final release of 4-aminophenol. Notably, the intermediate was not present in reactions catalyzed by Au_{25}NCs without protective ligands.

Metal NCs exhibit much higher electrocatalytic activity than bulk metal and larger NPs, and can hopefully provide low-cost, high-performance alternatives for commercial Pt catalysts in fuel cells [202]. In order to avoid potential side effects, *i.e.* blocking of mass transport and electron transfer, by the surface ligands of NCs and to enhance their stability, various carbon nanomaterials such as carbon nanotubes (CNTs) [203], carbon dots [204] and graphene [205] have been exploited as support materials of metal NCs. One-dimensional CNTs have been reported to form interconnected conducting networks capable of increasing the contact between loaded metal NCs and electrolytes as well as accelerating the electron transfer [206]. For example, electrocatalytically active CNT-PtNC composites were fabricated *via* homogenously

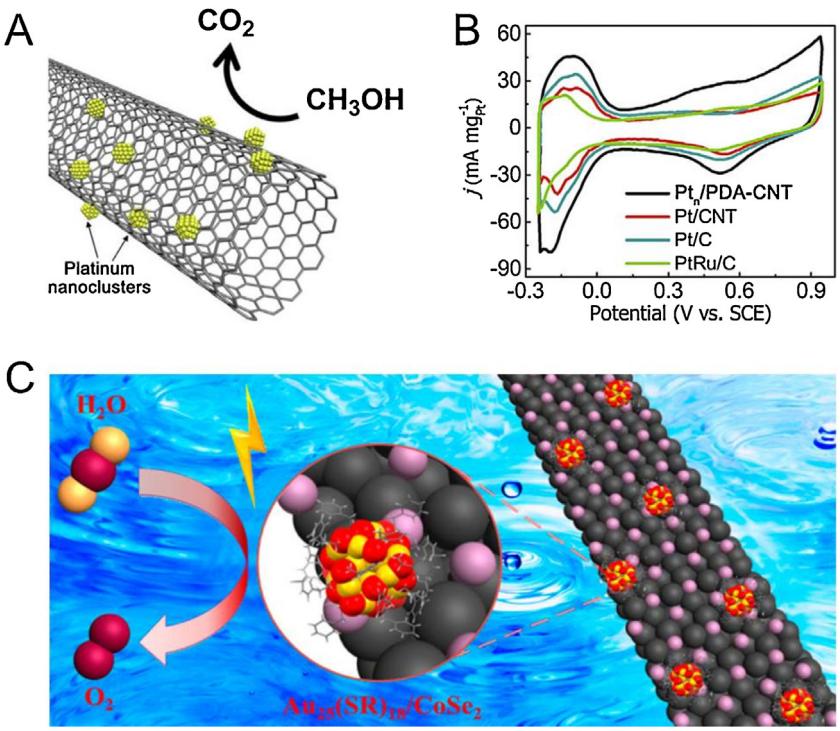

Fig. 20. (A) Schematic illustration of the structure of CNT-PtNC composites and (B) cyclic voltammetry of CNT-PtNC composites (denoted by "Pt_n/PDA-CNT" in the Fig.) *versus* other control Pt catalysts. Pt-CNT is a composite of CNT with PtNPs without polydopamine modification; Pt/C and PtRu/C are commercial catalysts. (C) Schematic illustration of $CoSe_2$-AuNC composites for electrocatalytic water oxidation. (Reproduced or adapted with permissions from Elsevier for (A) and (B), Ref. [207], and the American Chemical Society for (C), Ref [219]).

depositing ultradispersed PtNCs on polydopamine-functionalized CNTs (Fig. 20A) [207]. In comparison with other commercial Pt catalysts, these ultradispersed PtNCs feature a large accessible and active surface area, and a high fraction of surface atoms with low coordination numbers. The cyclic voltammetry curve of CNT-PtNC composites (Fig. 20B, black curve) displays a more pronounced hydrogen absorption/desorption response than other catalysts. These composites not only exhibit excellent mass activity and stability, but also show improved specific activity and CO tolerance for electrocatalytic methanol oxidation. A simple and sensitive non-enzymatic electrochemical sensor was developed based on dendrimer-encapsulated PtNCs and CNTs (PtNCs-CNTs) nanocomposites [208]. Due to synergistic effects between PtNCs and CNTs, the nanocomposites possessed excellent electron transfer properties, electron self-exchange and electrochemical catalytic activity on reduction of H_2O_2. Moreover, the sensor was successfully applied for real-time determination of extracellular H_2O_2 released from living cells. Tang, Chen and collaborators [209] described a novel *in-situ* reduction method to prepare ultrasmall PdNCs encapsulated in porous carbon nanosheet (CNS) composites. Their remarkably high electrocatalytic activity in the oxygen reduction reaction (ORR) can be attributed to the much greater effective surface area with respect to larger Pd particles [210]. Chang et al. [211] developed a "clean" method to synthesize PtNCs-graphene nanocomposites, in which polyvinyl-pyrrolidone (PVP) was chosen as surfactant to improve the dispersity of PtNCs on the graphene surface. Cyclic voltammetric and amperometric tests revealed that the synthesized nanocomposites exhibited excellent electrocatalytic activity toward glucose oxidation, suggesting a great potential in the fabrication of novel non-enzymatic glucose sensors. A new sensing layer composed of BSA-templated AuPt bimetallic NCs (AuPt NCs@BSA) and graphene nanoribbons was introduced for rapid, selective and sensitive detection of diazinon as an enzymeless electrochemical sensor [212].

Alternatively, AuNCs and other metal NCs (Pt, Pd) can also be directly grown on reduced GO (rGO) sheets without any additional protecting ligands [213]. These AuNCs-rGO hybrids displayed extraordinarily high catalytic activity in the ORR, with a comparable onset potential to commercial Pt/C catalysts but superior methanol tolerance and enhanced electrocatalytic stability. Compared with AuNPs-rGO hybrids, the small size of AuNCs benefits the activation of O_2. The decreased coordination of Au and the reduced electrophilicity of the NCs lower the activation energy barrier for the dissociative chemisorption of O_2, which facilitates its four-electron reduction and leads to a positive onset potential [214–217]. Moreover, the combination of AuNCs and rGO provides a synergistic effect for the enhanced ORR activity. A simple one-pot co-reduction method was developed to prepare well-dispersed AgPd alloyed NCs uniformly dispersed on rGO (AgPd NCs-rGO) at room temperature by utilizing 5-azacytosine as the capping agent [218]. Compared to commercial Pd/C (20 wt.%), these composites exhibited strongly enhanced catalytic effects in the reduction of 4-NP in the presence of $NaBH_4$. They retained a high catalytic efficiency even after seven cycles and their morphology was almost unchanged. These results suggest a noticeably enhanced stability and reusability of AgPd NCs-rGO.

Besides these carbon-based nanomaterials, other materials have also been exploited to hybridize with metal NCs for enhanced electrocatalytic applications. For example, atomically precise AuNCs were used to construct $CoSe_2$-AuNC composites for electrocatalytic water oxidation with an oxygen evolution reaction (OER) activity and durability in alkaline solution (Fig. 20C) [219]. The composites displayed a much reduced overpotential (~0.43 V at a current density of 10 mA cm^{-2}) compared to that of plain $CoSe_2$ (~0.52 V), which is attributed to the electronic interaction between AuNCs and $CoSe_2$ favoring formation of the OOH intermediate and desorption of O_2 in the OER process. Composites of Au_{25}NCs with MoS_2 nanosheets have also been fabricated for improving

the hydrogen evolution reaction (HER) performance *via* tailoring of their interfacial electronic interactions [168]. Defect-rich MoS_2 nanosheets possess abundant active edge sites and unsaturated sulfur atoms [220–222], and interfacial interactions between AuNCs and the MoS_2 defect sites could further enhance the HER activity. Recently, a novel nanocomposite based on the AgNC-decorated WS_2 nanosheets was developed, showing enhanced catalytic activity in the chemical and electrochemical reduction of H_2O_2[223]. The effect may be related to the difference in Fermi energy levels of the coupled nanomaterials, causing charge separation between the two components and creating highly active sites at the interface of the nanocomposite.

Conclusions and outlook

In this work, we have aimed at giving a comprehensive overview of recent research on metal NC-based nanocomposites. We have summarized different strategies used to synthesize these interesting composite materials and discussed diverse applications ranging from sensing and bioimaging to catalysis. Nanocomposites of metal NCs can easily be fabricated with diverse types of functional materials, *i.e.* biomolecules, carbon nanotubes, graphene, iron oxide NPs, silica and MOFs, most often by post-modifying pre-synthesized metal NCs *via* various strategies (*i.e.* chemical conjugation, electrostatic interaction, self-assembly, ligand exchange). Alternatively, it is also possible to generate metal NCs during the formation of composites in a single step, which is often simpler and more convenient.

Nevertheless, a number of challenges remain that need to be addressed for further improvement of the synthesis of metal NC-based nanocomposites. Firstly, the spatial dispersion of metal NCs within the nanocomposites greatly influences their application but is not yet well controllable in most syntheses. Thus, it will be important to further develop and refine more sophisticated synthesis procedures capable of precise control of the distribution of metal NCs as well as the structures of the resultant nanocomposites [224]. Secondly, in addition to monometallic NCs, the development of nanocomposites incorporating alloy metal NCs with different compositions should be further pursued. Alloy metal NPs show many interesting properties that are different from or better than those of monometallic NPs [225], offering new possibilities in their combination with other functional materials. Thirdly, although metal NC-based composites often show an enhanced luminescence QY with respect to plain metal NCs, there is still room for further improvement. This can be achieved by devising new or improved strategies either for the synthesis of highly luminescent metal NCs or for metal NC-based composites enhancing the emission of metal NCs. Fourthly, efforts will be worthwhile to balance the stoichiometric amount of each entity within a composite so as to achieve best performance in the intended application while minimizing the use of expensive materials. This issue will be particularly important for cost effectiveness and suppression of side effects in large-scale applications. Finally, industrial applications will inevitably lead to exposure of humans and other organisms to nanocomposites, either intentionally (*e.g.*, biomedical applications) or unintentionally (*e.g.*, environmental exposure). For their safe use, it will be important to elucidate their interactions with the biological environment (incorporation, biodistribution, in-vivo stability *etc.*) [226]. The physicochemical properties of metal NCs are typically retained within the nanocomposites and, sometimes, significantly enhanced properties of metal NCs can be observed. Moreover, nanocomposites often exhibit more functions than bare metal NCs owing to the introduction of additional components. These novel features can further broaden their utility in practical applications, for example, in sensing various biological/environmental analytes, in-vitro and in-vivo imaging as well as catalyzing important reactions. While we have focused our review on applications in these three areas, NC nanocomposites can also be put to good use in other areas such as energy and environment.

For example, AuNCs with molecule-like behavior have emerged as new light harvesters in energy conversion systems, *i.e.*, in solar cells [227,228]. Mesoscopic TiO_2 films modified with AuNCs were shown to deliver a stable photocurrent of 3.96 mA/cm^2 with a power conversion efficiency of 2.3% [227]. Opportunities exist to couple these metal NCs with plasmonic metal NPs to further increase the absorption range of the metal NC-sensitized solar cells in the future [229]. Recently, AuNCs have also been deposited on the surface of TiO_2 NPs for enhanced photocatalytic activity [230]. The AuNC-TiO_2 nanocomposites exhibited a twofold enhancement in photodegradation of organic pollutants (*i.e.*, methyl orange) and provide a good platform for the design of high performance photocatalysts for water treatment. Furthermore, metal NCs also possess many other interesting properties such as strong two-photon absorption [231], intrinsic chirality [232] and antibacterial activity [233], which are likely to be exploited in functional NC-based nanocomposites for optical and biomedical applications such as photodynamic therapy [234] and drug delivery [90,235] in the future.

Overall, metal NC-based nanocomposites have unique merits and hold great potential in a wide range of areas. Tremendous opportunities exist for further development of these novel materials by rational engineering. Progress in this fast-growing field will certainly yield more multifunctional composite materials and concomitantly spawn novel applications of metal NCs, making use of their unique physical and chemical properties.

Acknowledgements

L.S. acknowledges financial support from National Natural Science Foundation of China (NSFC, Grant No. 21705129), Shaanxi Natural Science Foundation (2018JM2004), the Fundamental Research Funds for the Central Universities (3102018jcc037, 3102019JC005) and Program of Introducing Talents of Discipline to Universities (B08040). G.U.N. was funded by the Helmholtz association, program Science and Technology of Nanosystems (STN).

References

[1] F.J. Heiligtag, M. Niederberger, Mater. Today 16 (2013) 262–271.
[2] Y. Xia, Angew. Chem. Int. Ed. 53 (2014) 12268–12271.
[3] B.A. Grzybowski, W.T.S. Huck, Nat. Nanotechnol. 11 (2016) 585–592.
[4] J.J. Wu, S.C. Liu, Adv. Mater. 14 (2002) 215–218.
[5] T.P. Yadav, R.M. Yadav, D.P. Singh, Nanosci. Nanotechnol. 2 (2012) 22–48.
[6] V. Subramanian, H. Zhu, R. Vajtai, P.M. Ajayan, B. Wei, J. Phys. Chem. B 109 (2005) 20207–20214.
[7] U.S. Mohanty, J. Appl. Electrochem. 41 (2011) 257–270.
[8] A.V. Kabashin, M. Meunier, J. Appl. Phys. 94 (2003) 7941–7943.
[9] S.H. Joo, S.J. Choi, I. Oh, J. Kwak, Z. Liu, O. Terasaki, R. Ryoo, Nature 412 (2001) 169–172.
[10] E. Roduner, Chem. Soc. Rev. 35 (2006) 583–592.
[11] R.A. Sperling, P. Rivera Gil, F. Zhang, M. Zanella, W.J. Parak, Chem. Soc. Rev. 37 (2008) 1896–1908.
[12] F.H. Liao, T.H. Wu, Y.T. Huang, W.J. Lin, C.J. Su, U.S. Jeng, S.C. Kuo, S.Y. Lin, Nano Lett. 18 (2018) 2864–2869.
[13] J.A. Hubbell, A. Chilkoti, Science 337 (2012) 303–305.
[14] S.M. Jafari, I. Katouzian, Crit. Rev. Microbiol. 44 (2018) 161–181.
[15] L. Liu, A. Corma, Chem. Rev. 118 (2018) 4981–5079.
[16] T. Pradeep, Anshup, Thin Solid Films 517 (2009) 6441–6478.
[17] A.F. Smith, S.E. Skrabalak, J. Mater. Chem. C 5 (2017) 3207–3215.
[18] B. Ni, Y. Shi, X. Wang,Adv. Mater. 30 (2018), 1802031.
[19] J. Zheng, P.R. Nicovich, R.M. Dickson, Annu. Rev. Phys. Chem. 58 (2007) 409–431.
[20] O. Varnavski, G. Ramakrishna, J. Kim, D. Lee, T. Goodson, J. Am. Chem. Soc. 132 (2010) 16–17.
[21] C. Gautier, T. Bürgi, J. Am. Chem. Soc. 128 (2006) 11079–11087.

[22] M. Zhu, C.M. Aikens, M.P. Hendrich, R. Gupta, H. Qian, G.C. Schatz, R. Jin, J. Am. Chem. Soc. 131 (2009) 2490–2492.
[23] Z. Wu, Angew. Chem. Int. Ed. 124 (2012) 2988–2992.
[24] L. Chen, C. Wang, Z. Yuan, H. Chang, Anal. Chem. 87 (2015) 216–229.
[25] J. Xu, L. Shang, Chin. Chem. Lett. 29 (2018) 1436–1444.
[26] J. Zhao, R. Jin, Nano Today 18 (2018) 86–102.
[27] Q. Gao, S. Xu, C. Guo, Y. Chen, L. Wang, ACS Appl. Mater. Interfaces 10 (2018) 16059–16065.
[28] M.A. Koklioti, N. Tagmatarchis, ChemNanoMat 2 (2016) 1065–1072.
[29] D.H. Hu, Z.H. Sheng, P.F. Zhang, D.Z. Yang, S.H. Liu, P. Gong, D.Y. Gao, S.T. Fang, Y.F. Ma, L.T. Cai, Nanoscale 5 (2013) 1624–1628.
[30] P. Zhao, K. He, Y. Han, Z. Zhang, M. Yu, H. Wang, Y. Huang, Z. Nie, S. Yao, Anal. Chem. 87 (2015) 9998–10005.
[31] Z. Wang, B. Chen, A.L. Rogach, Nanoscale Horiz. 2 (2017) 135–146.
[32] I. Chakraborty, T. Pradeep, Chem. Rev. 117 (2017) 8208–8271.
[33] Y. Tao, M. Li, J. Ren, X. Qu, Chem. Soc. Rev. 44 (2015) 8636–8663.
[34] L. Shang, S. Dong, G.U. Nienhaus, Nano Today 6 (2011) 401–418.
[35] Q. Yao, X. Yuan, T. Chen, D.T. Leong, J. Xie,Adv. Mater. 30 (2018), 1802751.
[36] R. Jin, C. Zeng, M. Zhou, Y. Chen, Chem. Rev. 116 (2016) 10346–10413.
[37] P. Zhang, J. Phys. Chem. C 118 (2014) 25291–25299.
[38] T. Chen, Q. Yao, R.R. Nasaruddin, J. Xie, Angew. Chem. Int. Ed. 58 (2019) 2–13.
[39] Q. Yao, T. Chen, X. Yuan, J. Xie, Acc. Chem. Res. 51 (2018) 1338–1348.
[40] R.R. Nasaruddin, T. Chen, N. Yan, J. Xie, Coord. Chem. Rev. 368 (2018) 60–79.
[41] A. Mooradian, Phys. Rev. Lett. 22 (1969) 185–187.
[42] M.B. Mohamed, V. Volkov, S. Link, M.A. El-Sayed, Chem. Phys. Lett. 317 (2000) 517–523.
[43] J. Zheng, C. Zhou, M. Yu, J. Liu, Nanoscale 4 (2012) 4073–4083.
[44] M.S. Devadas, J. Kim, E. Sinn, D. Lee, T. Goodson, G. Ramakrishna, J. Phys. Chem. C 114 (2010) 22417–22423.
[45] J. Sun, Y. Jin, J. Mater. Chem. C 2 (2014) 8000–8011.
[46] L. Shang, F. Stockmar, N. Azadfar, G.U. Nienhaus, Angew. Chem. Int. Ed. 52 (2013) 11154–11157.
[47] Z. Luo, X. Yuan, Y. Yu, Q. Zhang, D.T. Leong, J.Y. Lee, J. Xie, J. Am. Chem. Soc. 134 (2012) 16662–16670.
[48] Z. Wang, R. Chen, Y. Xiong, K. Cepe, J. Schneider, R. Zboril, C. Lee, A.L. Rogach,Part. Part. Syst. Charact. 34 (2017), 1700029.
[49] F. Xue, F. Qu, W. Han, L. Xia, J. You, Anal. Chim. Acta 1046 (2019) 170–178.
[50] Z. Wang, Y. Shi, X. Yang, Y. Xiong, Y. Li, B. Chen, W. Lai, A.L. Rogach,Adv. Funct. Mater. 28 (2018), 1802848.
[51] Z. Liu, W. Qi, G. Xu, Chem. Soc. Rev. 44 (2015) 3117–3142.
[52] Q. Zhai, J. Li, E. Wang, ChemElectroChem 4 (2017) 1639–1650.
[53] I. Díez, M. Pusa, S. Kulmala, H. Jiang, A. Walther, A.S. Goldmann, A.H.E. Müller, O. Ikkala, R.H.A. Ras, Angew. Chem. Int. Ed. 48 (2009) 2122–2125.
[54] L. Li, H. Liu, Y. Shen, J. Zhang, J. Zhu, Anal. Chem. 83 (2011) 661–665.
[55] M. Hesari, M.S. Workentin, Z. Ding, ACS Nano 8 (2014) 8543–8553.
[56] M. Zhao, A. Chen, D. Huang, Y. Zhuo, Y. Chai, R. Yuan, Anal. Chem. 88 (2016) 11527–11532.
[57] H. Jiang, X. Wang, Chin. J. Anal. Chem. 45 (2017) 1776–1785.
[58] M. Hesari, Z. Ding, Acc. Chem. Res. 50 (2017) 218–230.
[59] L. Shang, K. Nienhaus, G.U. Nienhaus, J. Nanobiotechnol. 12 (2014) 5.
[60] L. Shang, S. Brandholt, F. Stockmar, V. Trouillet, M. Bruns, G.U. Nienhaus, Small 8 (2012) 661–665.
[61] L. Shang, R.M. Dörlich, V. Trouillet, M. Bruns, G. Ulrich Nienhaus, Nano Res. 5 (2012) 531–542.
[62] H. Wang, R. Ma, K. Nienhaus, G.U. Nienhaus,Small 15 (2019), 1900974.
[63] H. Wang, Y. Lin, K. Nienhaus, G.U. Nienhaus, WIREs Nanomed. Nanobiotechnol. 10 (2017) 1500.
[64] P. Maffre, S. Brandholt, K. Nienhaus, L. Shang, W.J. Parak, G.U. Nienhaus, Beilstein J. Nanotechnol. 5 (2014) 2036–2047.
[65] P. Maffre, K. Nienhaus, F. Amin, W.J. Parak, G.U. Nienhaus, Beilstein J. Nanotechnol. 2 (2011) 374–383.
[66] C. Röcker, M. Pötzl, F. Zhang, W.J. Parak, G.U. Nienhaus, Nat. Nanotechnol. 4 (2009) 577–580.
[67] K. Anikin, C. Röcker, A. Wittemann, J. Wiedenmann, M. Ballauff, G.U. Nienhaus, J. Phys. Chem. B 109 (2005) 5418–5420.
[68] M. Kopp, S. Kollenda, M. Epple, Acc. Chem. Res. 50 (2017) 1383–1390.
[69] X. Jiang, A. Musyanovych, C. Röcker, K. Landfester, V. Mailänder, G.U. Nienhaus, Nanoscale 3 (2011) 2028–2035.
[70] L. Yang, L. Shang, G.U. Nienhaus, Nanoscale 5 (2013) 1537–1543.
[71] X. Jiang, B. Du, Y. Huang, J. Zheng, Nano Today 21 (2018) 106–125.
[72] C.Y. Tay, Y. Yu, M.I. Setyawati, J. Xie, D.T. Leong, Nano Res. 7 (2014) 805–815.
[73] G. Li, R. Jin, Acc. Chem. Res. 46 (2013) 1749–1758.
[74] S. Xie, H. Tsunoyama, W. Kurashige, Y. Negishi, T. Tsukuda, ACS Catal. 2 (2012) 1519–1523.
[75] J. Li, R.R. Nasaruddin, Y. Feng, J. Yang, N. Yan, J. Xie, Chem. Eur. J. 22 (2016) 14816–14820.
[76] Y. Wang, J. Chen, J. Irudayaraj, ACS Nano 5 (2011) 9718–9725.
[77] F. Su, S. Zhang, H. Ji, H. Zhao, J.Y. Tian, C.S. Liu, Z. Zhang, S. Fang, X. Zhu, M. Du, ACS Sens. 2 (2017) 998–1005.
[78] X.R. Song, N. Goswami, H.H. Yang, J. Xie, Analyst 141 (2016) 3126–3140.
[79] M.A. Habeeb Muhammed, T. Pradeep, Small 7 (2011) 204–208.
[80] X. Le Guével, B. Hötzer, G. Jung, M. Schneider, J. Mater. Chem. 21 (2011) 2974–2981.
[81] X. Wu, C. Li, S. Liao, L. Li, T. Wang, Z. Su, C. Wang, J. Zhao, C. Sui, J. Lin, Chem. Eur. J. 20 (2014) 8876–8882.
[82] M. Hembury, C. Chiappini, S. Bertazzo, T.L. Kalber, G.L. Drisko, O. Ogunlade, S. Walker-Samuel, K.S. Krishna, C. Jumeaux, P. Beard, C.S. Kumar, A.E. Porter, M.F. Lythgoe, C. Boissiere, C. Sanchez, M.M. Stevens, Proc. Natl. Acad. Sci. U. S. A. 112 (2015) 1959–1964.
[83] X. Yu, C. Zhang, L. Zhang, Y. Xue, H. Li, Y. Wu, Sens. Actuators B Chem. 263 (2018) 327–335.
[84] R. Tian, S. Zhang, M. Li, Y. Zhou, B. Lu, D. Yan, M. Wei, D.G. Evans, X. Duan, Adv. Funct. Mater. 25 (2015) 5006–5015.
[85] C. Wang, Y. Yao, Q. Song, J. Mater. Chem. C 3 (2015) 5910–5917.
[86] F. He, G. Yang, P. Yang, Y. Yu, R. Lv, C. Li, Y. Dai, S. Gai, J. Lin, Adv. Funct. Mater. 25 (2015) 3966–3976.
[87] A.H. Gröschel, A.H.E. Müller, Nanoscale 7 (2015) 11841–11876.
[88] X. Wang, C. Wang, N. Yang, J. Xia, L. Li, Colloid Surf. A 548 (2018) 27–31.
[89] X. Bai, S. Xu, L. Wang, Anal. Chem. 90 (2018) 3270–3275.
[90] A. Yahia-Ammar, D. Sierra, F. Merola, N. Hildebrandt, X. Le Guevel, ACS Nano 10 (2016) 2591–2599.
[91] W. Hou, F. Xia, G. Alfranca, H. Yan, X. Zhi, Y. Liu, C. Peng, C. Zhang, J.M. de la Fuente, D. Cui, Biomaterials 120 (2017) 103–114.
[92] C. Bosch-Navarro, Z.P.L. Laker, H.R. Thomas, A.J. Marsden, J. Sloan, N.R. Wilson, J.P. Rourke, Angew. Chem. Int. Ed. 54 (2015) 9560–9563.
[93] G. Wei, Z. Su, N.P. Reynolds, P. Arosio, I.W. Hamley, E. Gazit, R. Mezzenga, Chem. Soc. Rev. 46 (2017) 4661–4708.
[94] N. Habibi, N. Kamaly, A. Memic, H. Shafiee, Nano Today 11 (2016) 41–60.
[95] W. Zhang, D. Lin, H. Wang, J. Li, G.U. Nienhaus, Z. Su, G. Wei, L. Shang, Bioconjugate Chem. 28 (2017) 2224–2229.
[96] E.S. Shibu, S. Sugino, K. Ono, H. Saito, A. Nishioka, S. Yamamura, M. Sawada, Y. Nosaka, V. Biju, Angew. Chem. Int. Ed. 52 (2013) 10559–10563.
[97] M.A.H. Muhammed, P.K. Verma, S.K. Pal, R.C.A. Kumar, S. Paul, R.V. Omkumar, T. Pradeep, Chem. Eur. J. 15 (2009) 10110–10120.
[98] A. Caragheorgheopol, V. Chechik, Phys. Chem. Chem. Phys. 10 (2008) 5029–5041.
[99] M.J. Hostetler, A.C. Templeton, R.W. Murray, Langmuir 15 (1999) 3782–3789.
[100] S. Lin, N. Chen, S. Sum, L. Lo, C. Yang, Chem. Commun. (2008) 4762–4764.
[101] S.Y. Lin, N.T. Chen, S.P. Sun, J.C. Chang, Y.C. Wang, C.S. Yang, L.W. Lo, J. Am. Chem. Soc. 132 (2010) 8309–8315.
[102] R.A. Sperling, W.J. Parak, Philos. Trans. Math. Phys. Eng. Sci. 368 (2010) 1333–1383.
[103] M.B. Dickerson, K.H. Sandhage, R.R. Naik, Chem. Rev. 108 (2008) 4935–4978.
[104] J. Xie, Y. Zheng, J.Y. Ying, J. Am. Chem. Soc. 131 (2009) 888–889.
[105] K. Chaudhari, A. Baksi, T. Pradeep, Nano Rev. 3 (2012) 14767–14783.
[106] C. Liu, H. Wu, Y. Hsiao, C. Lai, C. Shih, Y. Peng, K. Tang, H. Chang, Y. Chien, J. Hsiao, J. Cheng, P. Chou, Angew. Chem. Int. Ed. 50 (2011) 7056–7060.
[107] C. Sun, Y. Yuan, Z. Xu, T. Ji, Y. Tian, S. Wu, J. Lei, J. Li, N. Gao, G. Nie, Bioconjugate Chem. 26 (2015) 193–196.
[108] C. Xu, Y. Wang, C. Zhang, Y. Jia, Y. Luo, X. Gao, Nanoscale 9 (2017) 4620–4628.
[109] G. Sun, L. Zhou, Y. Liu, Z. Zhao, New J. Chem. 37 (2013) 1028–1035.
[110] G. Liang, D. Ye, X. Zhang, F. Dong, H. Chen, S. Zhang, J. Li, X. Shen, J. Kong, J. Mater. Chem. B 1 (2013) 3545–3552.
[111] L. Han, J.M. Xia, X. Hai, Y. Shu, X.W. Chen, J.H. Wang, ACS Appl. Mater. Interfaces 9 (2017) 6941–6949.
[112] Q. Yuan, Y. Wang, L. Zhao, R. Liu, F. Gao, L. Gao, X. Gao, Nanoscale 8 (2016) 12095–12104.
[113] Y. Wang, Y. Cui, Y. Zhao, R. Liu, Z. Sun, W. Li, X. Gao, Chem. Commun. 48 (2012) 871–873.
[114] Y. Wang, Y. Cui, R. Liu, Y. Wei, X. Jiang, H. Zhu, L. Gao, Y. Zhao, Z. Chai, X. Gao, Chem. Commun. 49 (2013) 10724–10726.
[115] R. Huang, R. Liu, J. Mater. Sci. 52 (2017) 13455–13465.
[116] M.R. Jones, N.C. Seeman, C.A. Mirkin,Science 347 (2015), 1260901.
[117] Z. Chen, C. Liu, F. Cao, J. Ren, X. Qu, Chem. Soc. Rev. 47 (2018) 4017–4072.
[118] Z. Sun, Y. Wang, Y. Wei, R. Liu, H. Zhu, Y. Cui, Y. Zhao, X. Gao, Chem. Commun. 47 (2011) 11960–11962.
[119] J. Li, X. Zhong, F. Cheng, J.R. Zhang, L.P. Jiang, J.J. Zhu, Anal. Chem. 84 (2012) 4140–4146.
[120] K.P. Williams, X. Liu, T.N.M. Schumacher, H.Y. Lin, D.A. Ausiello, P.S. Kim, D.P. Bartel, Proc. Natl. Acad. Sci. U. S. A. 94 (1997) 11285–11290.
[121] H. Urata, K. Shinohara, E. Ogura, Y. Ueda, M. Akagi, J. Am. Chem. Soc. 113 (1991) 8174–8175.
[122] G. Han, Z. Jia, Y. Zhu, J. Jiao, D. Kong, X. Feng, Anal. Chem. 88 (2016) 10800–10804.
[123] M.E. Davis, Nature 417 (2002) 813–821.
[124] H. Jiang, Q. Lin, T. Akita, B. Liu, H. Ohashi, H. Oji, T. Honma, T. Takei, M. Haruta, Q. Xu, Chem. Eur. J. 17 (2011) 78–81.
[125] L. Liu, Y. Song, H. Chong, S. Yang, J. Xiang, S. Jin, X. Kang, J. Zhang, H. Yu, M. Zhu, Nanoscale 8 (2016) 1407–1412.
[126] L. Zhang, E. Wang, Nano Today 9 (2014) 132–157.
[127] G. Wang, G. Xu, Y. Zhu, X. Zhang, Chem. Commun. 50 (2014) 747–750.
[128] Y. Li, X. Hu, X. Zhang, H. Cao, Y. Huang, Anal. Chim. Acta 1024 (2018) 145–152.
[129] H. Liu, X. Zhang, X. Wu, L. Jiang, C. Burda, J. Zhu, Chem. Commun. 47 (2011) 4237–4239.
[130] Z. Yuan, M. Peng, Y. He, E.S. Yeung, Chem. Commun. 47 (2011) 11981–11983.
[131] X. Mu, L. Qi, P. Dong, J. Qiao, J. Hou, Z. Nie, H. Ma, Biosens. Bioelectron. 49 (2013) 249–255.
[132] S. Roy, G. Palui, A. Banerjee, Nanoscale 4 (2012) 2734–2740.
[133] Z. Bai, X. Ren, Z. Gong, C. Hao, Y. Chen, P. Wan, X. Meng, Chin. Chem. Lett. 28 (2017) 1901–1904.

[134] A. Bianchi-Smiraglia, M.S. Rana, C.E. Foley, L.M. Paul, B.C. Lipchick, S. Moparthy, K. Moparthy, E.E. Fink, A. Bagati, E. Hurley, H.C. Affronti, A.V. Bakin, E.S. Kandel, D.J. Smiraglia, M.L. Feltri, R. Sousa, M.A. Nikiforov, Nat. Methods 14 (2017) 1003–1009.
[135] Y. Yan, H. Yu, K. Zhang, M. Sun, Y. Zhang, X. Wang, S. Wang, Nano Res. 9 (2016) 2088–2096.
[136] C. Wang, Y. Huang, H. Lin, Z. Xu, J. Wu, M.G. Humphrey, C. Zhang, RSC Adv. 5 (2015) 61586–61592.
[137] L.E. Kreno, K. Leong, O.K. Farha, M. Allendorf, R.P. Van Duyne, J.T. Hupp, Chem. Rev. 112 (2012) 1105–1125.
[138] R.W. Huang, Y.S. Wei, X.Y. Dong, X.H. Wu, C.X. Du, S.Q. Zang, T.C.W. Mak, Nat. Chem. 9 (2017) 689–697.
[139] P. Huang, J. Lin, S. Wang, Z. Zhou, Z. Li, Z. Wang, C. Zhang, X. Yue, G. Niu, M. Yang, D. Cui, X. Chen, Biomaterials 34 (2013) 4643–4654.
[140] Y. Wang, X. He, W. Li, Y. Zhang, J. Mater. Chem. C 1 (2013) 2202–2208.
[141] Y. Chen, Y. Shen, D. Sun, H. Zhang, D. Tian, J. Zhang, J. Zhu, Chem. Commun. 47 (2011) 11733–11735.
[142] D. Yuan, S. Chen, R. Yuan, J. Zhang, W. Zhang, Analyst 138 (2013) 6001–6006.
[143] Y. Zhou, H. Wang, Y. Zhuo, Y. Chai, R. Yuan, Anal. Chem. 89 (2017) 3732–3738.
[144] Y. Yu, C. Lu, M. Zhang, Anal. Chem. 87 (2015) 8026–8032.
[145] H. Peng, H. Deng, M. Jian, A. Liu, F. Bai, X. Lin, W. Chen, Microchim. Acta 184 (2017) 735–743.
[146] Y. Yang, W. Wu, Q. Wang, H. Xiao, Y. Kuang, C. Liu, J. Electroanal. Chem. 772 (2016) 73–79.
[147] X.L. Zhang, X. Li, X.T. Li, Y. Gao, F. Feng, G.J. Yang, Sens. Actuators B Chem. 282 (2019) 927–935.
[148] L. Tang, J. Li, ACS Sens. 2 (2017) 857–875.
[149] H. Wei, E. Wang, Chem. Soc. Rev. 42 (2013) 6060–6093.
[150] X. Wang, Q. Wu, Z. Shan, Q. Huang, Biosens. Bioelectron. 26 (2011) 3614–3619.
[151] Y. Tao, Y. Lin, Z. Huang, J. Ren, X. Qu, Adv. Mater. 25 (2013) 2594–2599.
[152] Y. Tao, M. Li, B. Kim, D.T. Auguste, Theranostics 7 (2017) 899–911.
[153] S. Cho, H.Y. Shin, M.I. Kim,Biointerphases 12 (2017), 01A401.
[154] G.L. Wang, L.Y. Jin, X.M. Wu, Y.M. Dong, Z.J. Li, Anal. Chim. Acta 871 (2015) 1–8.
[155] G. Xu, L. Hu, Y. Yuan, L. Zhang, J. Zhao, S. Majeed, Anal. Chim. Acta 762 (2013) 83–86.
[156] L. Jin, Z. Meng, Y. Zhang, S. Cai, Z. Zhang, C. Li, L. Shang, Y. Shen, ACS Appl. Mater. Interfaces 9 (2017) 10027–10033.
[157] L.L. Wu, L.Y. Wang, Z.J. Xie, N. Pan, C.F. Peng, Sens. Actuators B Chem. 235 (2016) 110–116.
[158] C. Zheng, A. Zheng, B. Liu, X. Zhang, Y. He, J. Li, H. Yang, G. Chen, Chem. Commun. 50 (2014) 13103–13106.
[159] J. Li, X. Lin, Sens. Actuators B Chem. 124 (2007) 486–493.
[160] X. Gao, Y. Lu, M. Liu, S. He, W. Chen, J. Mater. Chem. C 3 (2015) 4050–4056.
[161] H. Dong, S. Jin, H. Ju, K. Hao, L. Xu, H. Lu, X. Zhang, Anal. Chem. 84 (2012) 8670–8674.
[162] Y. Si, Z. Sun, N. Zhang, W. Qi, S. Li, L. Chen, H. Wang, Anal. Chem. 86 (2014) 10406–10414.
[163] M. Pumera, A. Ambrosi, A. Bonanni, E.L.K. Chng, H.L. Poh, Trends Anal. Chem. 29 (2010) 954–965.
[164] J. Wang, X. Wang, S. Wu, J. Song, Y. Zhao, Y. Ge, C. Meng, Anal. Chim. Acta 906 (2016) 80–88.
[165] Y. Zhang, H. Liu, Z. Yang, S. Ji, J. Wang, P. Pang, L. Feng, H. Wang, Z. Wu, W. Yang, Anal. Methods 7 (2015) 6213–6219.
[166] Y. Wang, X. Bai, W. Wen, X. Zhang, S. Wang, ACS Appl. Mater. Interfaces 7 (2015) 18872–18879.
[167] P. Bollella, G. Fusco, C. Tortolini, G. Sanzò, G. Favero, L. Gorton, R. Antiochia, Biosens. Bioelectron. 89 (2017) 152–166.
[168] S. Zhao, R. Jin, Y. Song, H. Zhang, S.D. House, J.C. Yang, R. Jin,Small 13 (2017), 1701519.
[169] G. Yang, J. Shi, S. Wang, W. Xiong, L. Jiang, C. Burda, J. Zhu, Chem. Commun. 49 (2013) 10757–10759.
[170] D. Yue, M. Wang, F. Deng, W. Yin, H. Zhao, X. Zhao, Z. Xu, Chin. Chem. Lett. 29 (2018) 648–656.
[171] H. Dehong, S. Zonghai, F. Shengtao, W. Yanan, G. Duyang, Z. Pengfei, G. Ping, M. Yifan, C. Lintao, Theranostics 4 (2014) 142–153.
[172] J. Qiao, X. Mu, L. Qi, J. Deng, L. Mao, Chem. Commun. 49 (2013) 8030–8032.
[173] H. Chen, S. Li, B. Li, X. Ren, S. Li, D.M. Mahounga, S. Cui, Y. Gu, S. Achilefu, Nanoscale 4 (2012) 6050–6064.
[174] H. Jiang, G. Xu, Y. Sun, W. Zheng, X. Zhu, B. Wang, X. Zhang, G. Wang, Chem. Commun. 51 (2015) 11810–11813.
[175] Y. Kong, J. Chen, F. Gao, R. Brydson, B. Johnson, G. Heath, Y. Zhang, L. Wu, D. Zhou, Nanoscale 5 (2013) 1009–1017.
[176] Q. Zhuang, H. Jia, L. Du, Y. Li, Z. Chen, S. Huang, Y. Liu, Biosens. Bioelectron. 55 (2014) 76–82.
[177] X. Le Guével, N. Daum, M. Schneider,Nanotechnology 22 (2011), 275103.
[178] T. Zhao, X. He, W. Li, Y. Zhang, J. Mater. Chem. B 3 (2015) 2388–2394.
[179] T. Chen, Y. Hu, Y. Cen, X. Chu, Y. Lu, J. Am. Chem. Soc. 135 (2013) 11595–11602.
[180] Y. Chen, P. Chen, C. Wang, Y. Lin, C. Ou, L. Ho, H. Chang, Chem. Commun. 50 (2014) 8571–8574.
[181] K. Pyo, N.H. Ly, S.Y. Yoon, Y. Shen, S.Y. Choi, S.Y. Lee, S. Joo, D. Lee,Adv. Healthcare. Mater. 6 (2017), 1700203.
[182] X. Wu, X. He, K. Wang, C. Xie, B. Zhou, Z. Qing, Nanoscale 2 (2010) 2244–2249.
[183] Y. Wang, J. Chen, X. Yan, Anal. Chem. 85 (2013) 2529–2535.
[184] Y. Duan, R. Duan, R. Liu, M. Guan, W. Chen, J. Ma, M. Chen, B. Du, Q. Zhang, ACS Biomater. Sci. Eng. 4 (2018) 1055–1063.
[185] X. Chen, H. Zhu, X. Huang, P. Wang, F. Zhang, W. Li, G. Chen, B. Chen, Nanoscale 9 (2017) 2219–2231.
[186] J.F. Hainfeld, D.N. Slatkin, T.M. Focella, H.M. Smilowitz, Br. J. Radiol. 79 (2006) 248–253.
[187] C. Zhang, Z. Zhou, Q. Qian, G. Gao, C. Li, L. Feng, Q. Wang, D. Cui, J. Mater. Chem. B 1 (2013) 5045–5053.
[188] Y. Liu, G. Tian, X. He, W. Li, Y. Zhang, J. Mater. Chem. B 4 (2016) 1276–1283.
[189] R. Weissleder, M. Nahrendorf, Proc. Natl. Acad. Sci. U. S. A. 112 (2015) 14424–14428.
[190] E. Boros, E.M. Gale, P. Caravan, Dalton Trans. 44 (2015) 4804–4818.
[191] M. Engström, A. Klasson, H. Pedersen, C. Vahlberg, P.O. Käll, K. Uvdal, Magn. Reson. Mater. Phys. Biol. Med. 19 (2006) 180–186.
[192] S. Sun, L. Dong, Y. Cao, H. Sun, X. Yan, Anal. Chem. 85 (2013) 8436–8441.
[193] C.V. Durgadas, C.P. Sharma, K. Sreenivasan, Nanoscale 3 (2011) 4780–4787.
[194] X. Li, X. Zhang, X. Li, J. Chang, Cancer Bio. Med. 13 (2016) 339–348.
[195] P. Zhang, C. Chen, X. Kang, L. Zhang, C. Wu, J. Zhang, B. Han, Chem. Sci. 9 (2018) 1339–1343.
[196] S. Lu, Y. Hu, S. Wan, R. McCaffrey, Y. Jin, H. Gu, W. Zhang, J. Am. Chem. Soc. 139 (2017) 17082–17088.
[197] M. Mon, M.A. Rivero-Crespo, J. Ferrando-Soria, A. Vidal-Moya, M. Boronat, A. Leyva-Pérez, A. Corma, J.C. Hernández-Garrido, M. López-Haro, J.J. Calvino, G. Ragazzon, A. Credi, D. Armentano, E. Pardo, Angew. Chem. Int. Ed. 57 (2018) 6186–6191.
[198] Y. Jiang, X. Zhang, X. Dai, W. Zhang, Q. Sheng, H. Zhuo, Y. Xiao, H. Wang, Nano Res. 10 (2017) 876–889.
[199] G. Gao, Q. Xi, Y. Zhang, M. Jin, Y. Zhao, C. Wu, H. Zhou, P. Guo, J. Xu, Nanoscale 11 (2019) 1169–1176.
[200] L. Sun, Y. Yun, H. Sheng, Y. Du, Y. Ding, P. Wu, P. Li, M. Zhu, J. Mater. Chem. A 6 (2018) 15371–15376.
[201] R.R. Nasaruddin, T. Chen, J. Li, N. Goswami, J. Zhang, N. Yan, J. Xie, ChemCatChem 10 (2018) 395–402.
[202] W. Chen, S. Chen, Angew. Chem. Int. Ed. 121 (2009) 4450–4453.
[203] W. Yuan, J. Zhang, P.K. Shen, C.M. Li, S.P. Jiang, Electrochim. Acta 190 (2016) 817–828.
[204] M. Liu, W. Chen, Nanoscale 5 (2013) 12558–12564.
[205] K. Kwak, U.P. Azad, W. Choi, K. Pyo, M. Jang, D. Lee, ChemElectroChem 3 (2016) 1253–1260.
[206] Y. Xiao, W. Jiang, S. Wan, X. Zhang, J. Hu, Z. Wei, L. Wan, J. Mater. Chem. A 1 (2013) 7463–7468.
[207] H. Huang, Z. He, X. Lin, W. Ruan, Y. Liu, Z. Yang, Appl. Catal. A Gen. 490 (2015) 65–70.
[208] J.X. Liu, S.N. Ding, Sens. Actuators B Chem. 251 (2017) 200–207.
[209] W. Yan, Z. Tang, L. Li, L. Wang, H. Yang, Q. Wang, W. Wu, S. Chen, ChemElectroChem 4 (2017) 1349–1355.
[210] S. Zhao, H. Zhang, S.D. House, R. Jin, J.C. Yang, R. Jin, ChemElectroChem 3 (2016) 1225–1229.
[211] G. Chang, H. Shu, Q. Huang, M. Oyama, K. Ji, X. Liu, Y. He, Electrochim. Acta 157 (2015) 149–157.
[212] N. Pajooheshpour, M. Rezaei, A. Hajian, A. Afkhami, M. Sillanpää, F. Arduini, H. Bagheri, Sens. Actuators B Chem. 275 (2018) 180–189.
[213] H.J. Yin, H.J. Tang, D. Wang, Y. Gao, Z.Y. Tang, ACS Nano 6 (2012) 8288–8297.
[214] W. Tang, H. Lin, A. Kleiman-Shwarsctein, G.D. Stucky, E.W. McFarland, J. Phys. Chem. C 112 (2008) 10515–10519.
[215] W. Chen, S. Chen, Angew. Chem. Int. Ed. 48 (2009) 4386–4389.
[216] C. Jeyabharathi, S.S. Kumar, G.V. Kiruthika, K.L. Phani, Angew. Chem. Int. Ed. 49 (2010) 2925–2928.
[217] R. Pal, L.M. Wang, Y. Pei, L.S. Wang, X.C. Zeng, J. Am. Chem. Soc. 134 (2012) 9438–9445.
[218] X.Y. Zhu, Z.S. Lv, J.J. Feng, P.X. Yuan, L. Zhang, J.R. Chen, A.J. Wang, J. Colloid Interface Sci. 516 (2018) 355–363.
[219] S. Zhao, R. Jin, H. Abroshan, C. Zeng, H. Zhang, S.D. House, E. Gottlieb, H.J. Kim, J.C. Yang, R. Jin, J. Am. Chem. Soc. 139 (2017) 1077–1080.
[220] T.F. Jaramillo, K.P. Jørgensen, J. Bonde, J.H. Nielsen, S. Horch, I. Chorkendorff, Science 317 (2007) 100–102.
[221] J. Xie, H. Zhang, S. Li, R. Wang, X. Sun, M. Zhou, J. Zhou, X.W. Lou, Y. Xie, Adv. Mater. 25 (2013) 5807–5813.
[222] Y. Yan, B. Xia, X. Ge, Z. Liu, J.Y. Wang, X. Wang, ACS Appl. Mater. Interfaces 5 (2013) 12794–12798.
[223] A. Khataee, M. Haddad Irani-nezhad, J. Hassanzadeh, S. Woo Joo, J. Colloid Interface Sci. 515 (2018) 39–49.
[224] A. Sánchez-Iglesias, N. Claes, D.M. Solís, J.M. Taboada, S. Bals, L.M. Liz-Marzán, M. Grzelczak, Angew. Chem. Int. Ed. 130 (2018) 3237–3240.
[225] R. Ferrando, J. Jellinek, R.L. Johnston, Chem. Rev. 108 (2008) 845–910.
[226] R. Zellner, J. Blechinger, C. Bräuchle, I. Hilger, A. Janshoff, J. Lademann, V. Mailänder, M.C. Meinke, G.U. Nienhaus, A. Patzelt, F. Rancan, B. Rothen-Rutishauser, R.H. Stauber, A.A. Torrano, L. Treuel, A. Vogt, Biological Responses to Nanoparticles, Handbook of Clinical Nanomedicine: Law, Business, Regulation, Safety, and Risk, 2016, pp. 745–808.
[227] Y.S. Chen, H. Choi, P.V. Kamat, J. Am. Chem. Soc. 135 (2013) 8822–8825.

[228] M.A. Abbas, T.Y. Kim, S.U. Lee, Y.S. Kang, J.H. Bang, J. Am. Chem. Soc. 138 (2016) 390–401.
[229] J. Li, S.K. Cushing, F. Meng, T.R. Senty, A.D. Bristow, N. Wu, Nat. Photonics 9 (2015) 601–607.
[230] H. Zhu, N. Goswami, Q. Yao, T. Chen, Y. Liu, Q. Xu, D. Chen, J. Lu, J. Xie, J. Mater. Chem. A 6 (2018) 1102–1108.
[231] G. Ramakrishna, O. Varnavski, J. Kim, D. Lee, T. Goodson, J. Am. Chem. Soc. 130 (2008) 5032–5033.
[232] S. Knoppe, T. Bürgi, Acc. Chem. Res. 47 (2014) 1318–1326.
[233] K. Zheng, M.I. Setyawati, D.T. Leong, J. Xie, ACS Nano 11 (2017) 6904–6910.
[234] D. Yang, A. Gulzar, G. Yang, S. Gai, F. He, Y. Dai, C. Zhong, P. Yang,Small 13 (2017), 1703007.
[235] D. Chen, Z. Luo, N. Li, J.Y. Lee, J. Xie, J. Lu, Adv. Funct. Mater. 23 (2013) 4324–4331.

Li Shang received his B.S. (2004) from Wuhan University and his Ph.D. in Chemistry (2010, supervisor: Prof. Shaojun Dong) from Changchun Institute of Applied Chemistry, Chinese Academy of Sciences. In 2010, he joined the group of Prof. G. Ulrich Nienhaus, Karlsruhe Institute of Technology (KIT), Germany, as a Humboldt fellow and then as a Research Associate. In 2016, he became a Professor in the School of Materials Science and Engineering, Northwestern Polytechnical University, China. His research interests are focused on the design and synthesis of luminescent nanomaterials for biological applications.

Jie Xu is a graduate student at the School of Materials Science and Engineering, Northwestern Polytechnical University, China. She received her master degree in Analytical Chemistry from Dalian University of Technology in 2016. Currently, she is pursuing her PhD degree under the supervision of Dr. Li Shang, working on the development of functional luminescent metal nanoclusters for bioimaging applications.

Gerd Ulrich Nienhaus studied Physics and Physical Chemistry at the University of Münster, Germany, where he received his PhD degree in 1988. In 1990, he joined the Department of Physics at the University of Illinois at Urbana-Champaign, USA, where he is still appointed as an Adjunct Professor. In 1996, he became Professor and Director of the Institute of Biophysics at the University of Ulm, Germany. In 2009, he accepted a position as a Professor and Director of the Institute of Applied Physics at the Karlsruhe Institute of Technology (KIT), Germany. His interdisciplinary research ranges from the development of advanced optical microscopes *via* luminescence marker development to fundamental molecular and cellular biophysics.